PONTIFICIA UNIVERSIDAD CATÓLICA DE CHILE
ESCUELA DE INGENIERÍA

EXPERIMENTAL AND NUMERICAL CHARACTERIZATION OF A SIX-BLADE TIDAL TURBINE

CLEMENTE MAURICIO GOTELLI ALVIAL

Thesis submitted to the Office of Research and Graduate Studies
in partial fulfillment of the requirements for the degree of
Master of Science in Engineering

Advisor:
CRISTIÁN ESCAURIAZA

Santiago de Chile, November 2018

PONTIFICIA UNIVERSIDAD CATÓLICA DE CHILE
ESCUELA DE INGENIERÍA

EXPERIMENTAL AND NUMERICAL CHARACTERIZATION OF A SIX-BLADE TIDAL TURBINE

CLEMENTE MAURICIO GOTELLI ALVIAL

Members of the Committee:
CRISTIÁN ESCAURIAZA
WERNHER BREVIS
OSCAR LINK
LUIS CIFUENTES

Thesis submitted to the Office of Research and Graduate Studies
in partial fulfillment of the requirements for the degree of
Master of Science in Engineering

Santiago de Chile, November 2018

To my mother, my siblings, and

Cande

ACKNOWLEDGEMENTS

First of all, I would like to thank my family for their constant support, without which this work would not have been possible. This work is dedicated in a special way to my mother, Esther, to whom I thank for her enormous effort and dedication throughout my life, especially in the most difficult moments that we had to overcome as a family. The time to thank you will never be enough because I know how difficult it was. I also thank my brother, Marco, and my sister, Cata, who have looked after me throughout my life as if I were more a son than a brother. Thank you for making our family a solid and happy core. The family is first, always.

I would like to thank Candei for everything. Thank you for your concern, for your love, and for getting the best out of me. Since I met you I have become a better person, and I will thank you forever. Without your support I would never have reached this point, you have convinced me that I am capable, and you have supported me in every decision I have made, always with a lot of love and giving joy to my life. I could not stop mentioning the Retamal Martínez family, especially Lolo and Totó, who have welcomed me as one of the family and have treated me with great affection from the moment I met them.

I would also acknowledge the Environmental Fluid Mechanics group: Jorge, Kari, Dani, Rosario and Maida. Thank you for being good friends and co-workers through all these years. ”Let no men separate what science has joined”. In a special way, I would like to thank my advisor, Cristián Escauriaza. Thank you for trusting me, and my abilities. Thank you for being like a friend and at the same time a good guide.

Work supported by Chile's Marine Energy Research & Innovation Center (MERIC) CORFO project 14CEI2-28228. Powered@NLHPC: This research was partially supported by the supercomputing infrastructure of the NLHPC (ECM-02)

TABLE OF CONTENTS

LIST OF FIGURES

LIST OF TABLES

ABSTRACT

Marine hydrokinetic (MHK) turbines are developed to harness the energy of currents in tidal channels. Before installing multiple devices in underwater arrays it is necessary to understand the interactions with the environment and with other MHK turbines located in their wake, to study the changes of the local flow hydrodynamics, the total power that can be extracted, and its variability. In this investigation we experimentally analyze the wake flow and power generation statistics of the scaled model of a Sabella D10 turbine for two different cases: a single turbine, and an array of two turbines aligned. In addition, we perform 3D numerical simulations of these cases by using a Blade Element Momentum Actuator Disk (BEM-AD) model for the turbines, coupled with the detached-eddy simulation (DES) approach for the flow, to predict the effects of these two cases and provide insights on the characteristics of the mean flow and the dynamics of turbulent coherent structures. The results show a good agreement in mean velocity statistics and sediment dynamics between the model and experimental measurements. Power coefficients obtained from simulations show a decrease in the average and an increase in variability when the flow turbulent intensity upstream the turbine increases. We also provide a detailed description of the flow past horizontal-axis MHK turbines, and the changes on the local flow dynamics using a numerical model with a low computational cost, emphasizing the effects on the turbulent statistics, the performance of the devices, the base design effect on the flow, and scour mechanisms.

Keywords: tidal turbines, marine energy, Acoustic Doppler Velocimeter, DES, BEM, velocity deficit, scour.

RESUMEN

Las turbinas marinas hidrocinéticas (MHK, por sus siglas en inglés) son desarrolladas para aprovechar la energía de las corrientes en canales de mareas. Antes de instalar múltiples dispositivos en arreglos submarinos, es necesario entender las interacciones con el ambiente y con otras turbinas MHK ubicadas en su estela, para estudiar los cambios locales de la hidrodinámica del flujo, la potencia total que puede ser extraída, y su variabilidad. En esta investigación analizamos experimentalmente el flujo de la estela y los estadísticos de la generación de potencia del modelo escalado de una turbina D10 de Sabella para dos casos distintos: una turbina solitaria y un arreglo de dos turbinas alineadas. Además, realizamos simulaciones numéricas en 3D de estos casos usando un modelo *Blade Element Momentum Actuator Disk* (BEM-AD) para la representación de las turbinas, acoplado con un modelo *Detached-eddy simulation* (DES) para resolver el flujo, para predecir los efectos de estos dos casos y proveer avances de las características del flujo medio y las dinámicas de las estructuras coherentes turbulentas. Los resultados muestran un buen ajuste en los estadísticos de velocidad media y dinámica de sedimentos entre el modelo y las mediciones experimentales. Los coeficientes de potencia obtenidos de las simulaciones muestran una disminución en la media y un aumento en la variabilidad para la potencia y el empuje cuando la intensidad turbulenta del flujo aguas arriba de la turbina aumenta. También entregamos una descripción detallada del flujo pasado las turbinas, y los cambios en la dinámica local del flujo usando un modelo numérico con bajo costo computacional, enfatizando los efectos en los estadísticos de la turbulencia, el rendimiento de los dispositivos, el efecto del diseño de la base sobre el flujo, y los mecanismos de erosión.

Palabras Claves: turbinas de corriente, energías marinas, Velocímetro acústico Doppler, DES, BEM, deficit de velocidad,socavación.

1. INTRODUCTION

Fossil fuels, e.g. coal, petroleum oil and natural gas, have largely powered world development in the past two centuries (Khojasteh, Mousavi, Glamore, & Iglesias, 2018). Even though is well known that these energy sources produce air pollution and contribute to climate change, most of electricity demand is still being supplied by fossil fuels (Valente, Iribarren, & Dufour, 2017). According to the International Energy Outlook 2016 reference case, renewable energies will represent nearly a 30% of global net electricity generation by 2040 (U.S. Energy Information Administration, 2016). In order to overcome this percentage, new technologies and research are needed.

Oceans represent a vast source of different renewable energies. In general, ocean energy can be divided into six types of different origin and characteristics: ocean wave, tidal range, tidal current, ocean current, ocean thermal energy, and salinity gradient (The Executive Committee of Ocean Energy Systems, 2015). Tidal current is one of the most explored technologies due to the fact that marine hydrokinetic (MHK) tidal turbines convert kinetic energy to electricity using relatively mature technologies, similar to wind turbines (Zhou, Benbouzid, Charpentier, Scuiller, & Tang, 2017). Tidal current energy is expected to play a major role in meeting future energy needs due to its relative advantages to other renewable energies. The astronomic-driven nature of tides is determined by the gravitational interaction of the earth with the sun and moon, this makes marine tidal currents highly predictable with 98% accuracy for decades (Vazquez & Iglesias, 2015) and makes them a perfect complement to other renewable energies like solar panels.

Different types of MHK turbines designs have been developed and tested during the last years (Rourke, Boyle, & Reynolds, 2010; Lewis, Neill, Robins, & Hashemi, 2015). From all alternatives, Horizontal Axis Tidal Turbines (HATTs) are the front-runners, concentrating most of the research and investments in the sector (Magagna & Uihlein, 2015; Yuce & Muratoglu, 2015). There are several horizontal axis turbine technologies, the majority of them have now achieved megawatt-level power capacity and have been chosen

by some leading industrial consortiums to build pilot demonstrative MHK turbine farms which are the final step before the final commercial stage (Zhou et al., 2017). A general characterization of all the different alternatives being tested is that they have a power capacity from 1 to 2 MW; the corresponding rated current velocities are from 2.6 to 4.0 m/s, and the maximum turbine power coefficient, Cp, values are estimated from 0.34 to 0.45 (Zhou et al., 2017).

In the final commercial stage all turbine models will be placed in farms, analogously to wind turbines. Even though it is unquestionable that the deployment of this devices in arrays will have an impact over the environment (Nash & Phoenix, 2017), the specific effects of implementing these technologies are not completely clear yet. In order to understand the impacts of deploying real scale prototypes, and how turbines interact with each other, changing their performance, it is necessary to use different tools like numerical modeling, field work, and laboratory experiments, by doing so it is possible to completely describe the flow dynamics and the influence of this devices over the surrounding environment.

In the last years, several experimental studies has been performed by different authors, mostly on single turbine cases, in order to further the understanding of device-flow interactions. For example, Chamorro et al. (2013, 2015) examined the effects of upstream turbulence and energetic coherent motions on turbine response and their effects on wake recovery. They showed that the response is coupled to upstream turbulence below a critical rotation frequency and uncoupled at higher frequencies, and that wake recovery was related to the tip vortices breakdown and other large motions. Maganga et al. (2010) studied the influence of ambient turbulence intensity on the turbine performance and wake characterization, and found out that for an incoming flow with a greater ambient turbulence intensity there are higher loading fluctuations on the blades. Mycek et al. (2013, 2014b) studied the turbulence intensity effects on marine current turbines behavior; single and two interacting turbines. They showed, while the mean turbine power performance remains stable in time, that performance fluctuations increase dramatically with turbulent

intensity. Their work also showed that wake shape, and length largely depend on the upstream turbulence intensity.

Experiments with scaled turbines are limited to laboratory flows as these can cover only a limited range of operating conditions and are subject to scale effects (Apsley, Stallard, & Stansby, 2018). As in laboratory or in the field it is impossible to simultaneously have data for the entire spatial and temporal domain, the use of numerical modeling as a complementary tool is needed as it gives complete information in both aspects. The variety of alternatives to model turbines and its wake characteristics differs on the demand of computational resources, offering also a wide range of precision. Current modeling strategies range from simpler computationally inexpensive models that solve the flow in steady-state. Other approaches consider turbines as uniformly-loaded disks, and more complex, highly accurate and computationally expensive models like Large Eddy Simulation (LES) for solving the flow with a complete turbine geometry representation.

It has been recognized that LES is the best method for simulating near-field wake flows while Unsteady Reynolds-averaged Navier–Stokes (URANS) methods based on isotropic turbulence models are not suitable due to the observed anisotropy of the Reynolds stresses (Tedds, Owen, & Poole, 2014). Nevertheless, as full resolution simulations of the rotor are cost-prohibitive, LES is not practical for modeling turbine arrays, due to current hardware capabilities (Bowman et al., 2018). Therefore, alternative strategies can be used such as the actuator disk model (ADM) (Batten, Harrison, & Bahaj, 2013; Gebreslassie et al., 2016; Rao, Xue, Bao, & Funke, 2016; Shives & Crawford, 2016; Koh & Ng, 2017). Other alternatives include the blade element momentum model (BEM) (Allsop, Peyrard, Thies, Boulougouris, & Harrison, 2017; Edmunds, Williams, Masters, & Croft, 2017; Abutunis, Hussein, & Chandrashekhara, 2018; Rahimian, Walker, & Penesis, 2018), and the actuator lines model (ALM) (Ahmadi, 2018; Apsley et al., 2018).

Blade Element Momentum is an analytical approach, originally derived from Glauert's propeller theory (Edmunds et al., 2017), which uses tabulated airfoil data to incorporate rotational components into the flow. The method considers the global effects caused by

the turbine blades onto an actuator volume. This technique is widely used in the wind turbine industry and the obtained results have proven to be in good agreement with experimental measurements (Burton, Jenkins, Sharpe, & Bossanyi, 2011). During the last years this method has also been applied to MHK turbines (Masters, Chapman, Willis, & Orme, 2011). However, as Kang et al. (2014) states, the lack of details of the full turbine geometry does not produce essential vortical structures that dominate the evolution of turbine wakes. This include blade tip vortices (Schluntz & Willden, 2015) and the downstream wake meandering phenomenon (Li & Çalişal, 2010). This limitations can be corrected by taking into account the loss of momentum caused by the tip within the numerical model (Shen, Mikkelsen, Sørensen, & Bak, 2005). A similar approach can be follow for other effects not considered in the basic BEM, such as yawed rotors, hub losses, or heavily loaded rotors.

In this study a BEM model coupled with a Detached Eddy Simulation (DES) flow solver is used. DES is a hybrid Computational Fluid Dynamics (CFD) solver that uses RANS equations near wall boundaries to save computational resources, while in more complex areas that contains vortical structures of interest, it uses a LES approach. This solver has been employed to solve a variety of turbulent flows in a wide range of Reynolds numbers. The model has been successfully compared to experimental observations of different type of flows (Paik et al., 2010; Escauriaza & Sotiropoulos, 2011a). In the work developed by Gajardo et al. (submitted 2018) a DES solver coupled with BEM was used to numerically study three 3-bladed turbines configurations that were formerly characterized by Stallard et al. (2013a). The comparison with experimental results showed a better performance than RANS simulations using a detailed geometry. This shows that BEM approach is a valid alternative when is used along with a detailed turbulence flow solver like DES.

The objective of the present study is to characterize a 6-bladed turbine, the D10 of Sabella, as a single turbine centered in a flume. The work also focus on the analysis of the turbulence characteristics of two turbines in tandem. The DES-BEM numerical

analysis are also complemented and validated using experimental results obtained in a tilting bed flume with an erodible bed. Turbine-flow-environment interaction will be studied from experiments and simulations considering mean and instantaneous flow statistics, performance coefficients, and experimental measurements of scouring and deposition in laboratory. This thesis is organized as follows, section 2 explains the methodology for laboratory experiments and numerical simulations using the DES-BEM model. Section 3 presents and compare numerical model results and experimental measurements. Finally, Section 5 states the concluding remarks and future research work.

2. MATERIALS AND METHODS

The prototype used for this study is the D10 model of Sabella, a bidirectional hydrokinetic horizontal axis tidal turbine (HATT) that was the first tidal turbine to produce electricity and be connected to the power grid (Paboeuf et al., 2016). The model is a six-bladed turbine -unlike the typically used three-bladed turbine models-, 10 m rotor diameter, 17 m high, 450 tons in weight, and 0.5-1.1MW power capacity at speeds of current of 3.0-4.0 m/s (Zhou, Scuiller, Charpentier, Benbouzid, & Tang, 2014). The turbine consists of two parts, the upper part is the turbine itself, formed by the rotor and hub; and the lower part is the support structure, which consists of three gravitational foundations that gives stability and seabed anchorage for the turbine (Paboeuf et al., 2016). Recently, one of these turbines has been deployed for the second time at the Fromveur passage (near Brest) in France at 55 m deep (Zhou et al., 2017).

2.1. Experimental setup

We carried out the experimental measurements in the tilting bed flume of the Saint Anthony Falls Laboratory (SAFL) at the University of Minnesota. The channel has dimensions of 14.6 m long and 0.9 m wide, slope variability from -1% to 6% that we set at 0.1%, a recirculation system for the quartz sediment moving bed ($d_{50} = 0.0018$m), and a 3-axis flume-transversing Data Acquisition (DAQ) Carriage showed in Figure 2.1. We set the water height, h, at 0.3m in order to have similarity of Froude (Fr) between the scale model and the operation conditions of the turbine prototype, the other main dimensionless parameters (e.g. Reynolds and Tip Speed Ratio (TSR)) remain in similar ranges. Under these conditions the values of local shear stress were below critical value according to the Shields curve and sediment critical mobility parameter (van Rijn, 1984). Therefore all experiments were made with clear water conditions, which was corroborated empirically before each measurement.

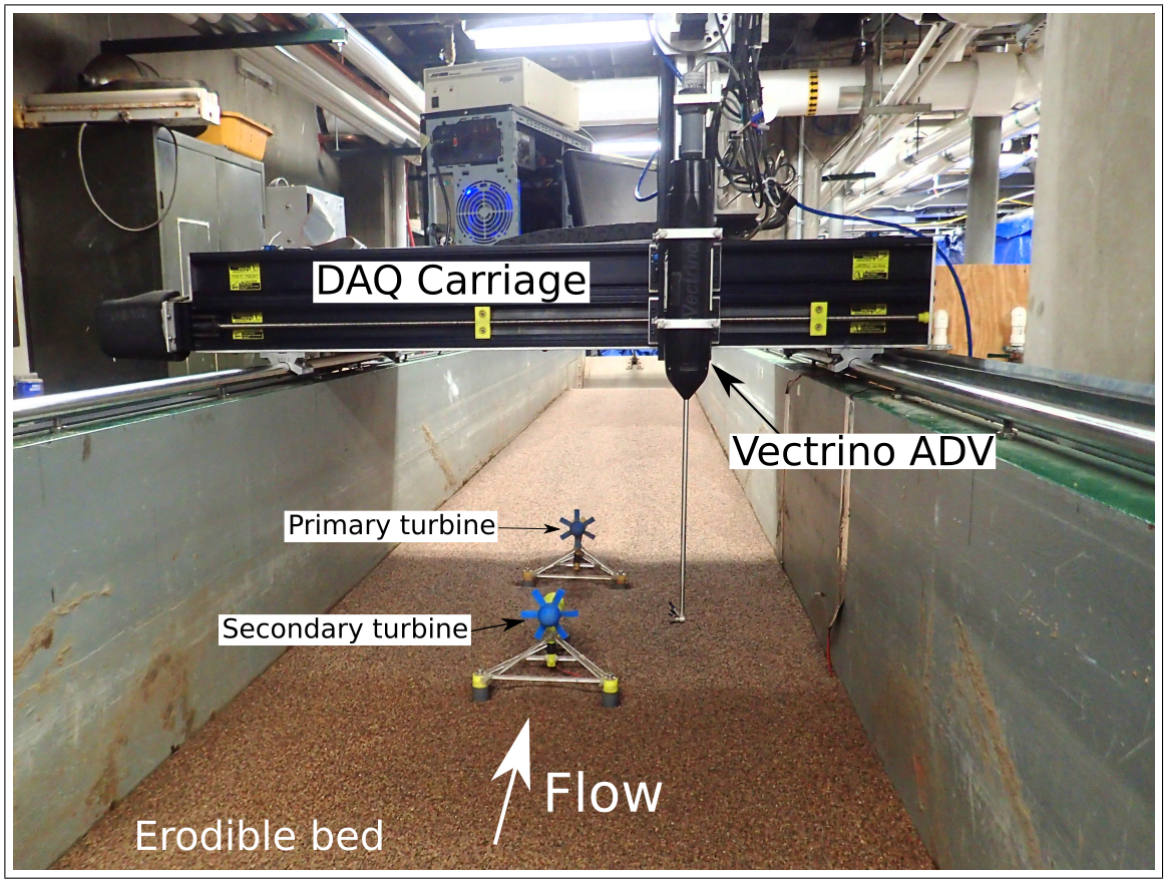

Figure 2.1. Flume setup for TT case. Both turbines are aligned and centered. Side-looking Nortek ADV velocimeter is mounted on the DAQ Carriage.

The turbine scaled model used in our experiments was an ABS plastic 3D-printed turbine with a scale of 1:108 based on the original plans of the prototype obtained from Sabella. The turbines were equipped with an isolated miniature DC motor for instantaneous voltage measurement. The proper torque of the DC motor allowed to have values of tip-speed ratio (TSR) near to the indicated by design of the prototype. The turbine produced a cross section blockage of 2.5%, so blocking effects are negligible according to previously reported blockage studies (Nishino & Willden, 2012; Chamorro et al., 2013). Table 2.1 summarizes the main turbine and flow characteristics.

We performed velocity, scour, and voltage measurements for two different cases: a single turbine (ST) centered at transverse section, and two turbines (TT) also centered,

Table 2.1. Primary turbine and flow characteristics for both study cases

Parameter	Definition	ST	TT	Unit
D	Diameter	0.092	0.092	m
D_h	Hub diameter	0.02	0.02	m
h_h	Hub height	0.010	0.010	m
N_b	Number of blades	6	6	-
Re	Reynolds number	126,667	126,667	-
Fr	Froude number	0.24	0.24	-
U_∞	Upstream velocity	0.42	0.42	m·s^{-1}
Ω	Rotor rotational velocity	16.6	12.4	rad·s^{-1}
TSR	Tip-speed ratio	3.65	2.01	-

aligned and separated by 6 turbine diameters ($6D = 55$ cm) measured from the hub end of the upstream turbine to the nacelle of the downstream turbine. In the ST case the turbine was located 7 m downstream of the channel flow inlet. For the TT case the downstream turbine (hereafter referred to as the primary turbine) was kept in the same place, while the secondary turbine was located 6D upstream. We chose turbines position to be within a domain where the flow is developed, and the topography is not influenced by the channel edge conditions. We define the origin of the coordinate system ($(X, Y, Z) = (0, 0, 0)$) at the hub end of the primary turbine, coincident with the rotor center.

We used two Nortek Vectrino ADV devices (top and side looking) to measure velocity at different flume positions. Before each measurement we positioned the Vectrino 2 m (approximately $20D$) upstream of the secondary turbine to obtain the inflow profile without the perturbation caused by the turbine presence. At the center of the channel, for the first three diameters of the wake, counted from the origin of the coordinate system, we measured vertical velocity profiles composed by nine different points separated by 2 cm in vertical direction. The center of this profiles was coincident with the hub height (h_h). In the transverse direction we measured the velocity for three profiles of nine points contained within the turbine rotor. The velocity deficit caused by the turbine effect was registered in the longitudinal direction. We measured the longitudinal velocity at hub height within the first ten diameters. We measured the velocity at each point for 3 minutes at a sample rate

of 200 Hz in all points where the average velocity was needed. The flow energy spectra was obtained from velocity measurements taken for 15 minutes at hub height in two different locations: 2 m upstream and 10D downstream of primary turbine. We filtered all the instantaneous velocity data obtained on this measurements using the spikes removal technique proposed by Parsheh et al. (2010). A schematic representative of both arrays and points measured is shown in Figure 2.2.

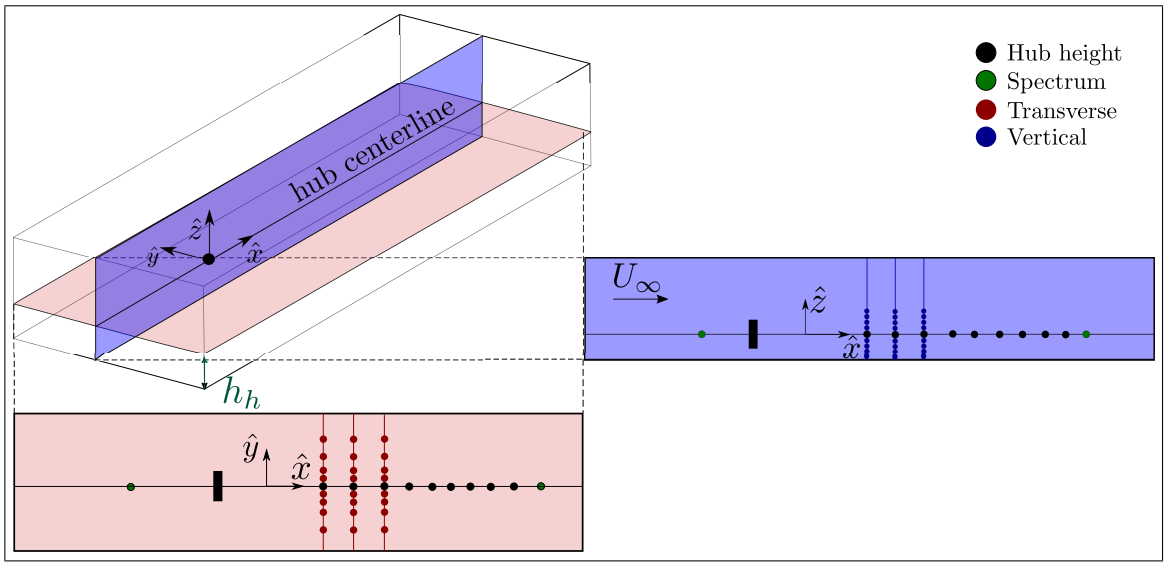

Figure 2.2. Points measured for both cases. Black: hub height (h_h) for deficit at centerline, green: long exposure for energy spectrum, red: transverse profiles, blue: vertical profiles. U_∞ indicates flow direction. Disk on this image represents primary turbine.

In both study cases a Measurement Computing MiniLAB 1008 USB data acquisition board recorded voltage at a rate of 200 Hz only for the main turbine during all the time we were taking measurements. By means of a Fast Fourier Transform (FFT) analysis of the instantaneous voltage record, representative indicators of performance and turbine operation can be obtained. In the resulting spectra, peaks and their resonants indicates the turbine rotation frequency (Hill, Musa, & Guala, 2016) and how it responds to flow variations caused by structures present upstream.

MHK turbines interact with their surroundings and produce alterations in local dynamics of sediment transport and deposition (Hill, Musa, Chamorro, Ellis, & Guala, 2014; Hill et al., 2016; Musa, Hill, Sotiropoulos, & Guala, 2018). We recorded the channel bed topography alterations produced by the interaction with both turbines every 2mm by using a Keyence LK-500 laser mounted on the DAQ Carriage. In order to estimate transport capacity from the DES-BEM model, we evaluated the shear velocity (u_*) as a sediment transport capacity indicator. The latter is defined as:

$$u_* = \sqrt{\frac{\tau}{\rho}} \tag{2.1}$$

where τ is the bed shear stress often defined as $\tau = \gamma R S_0$ (Julien, 2010), R is the hydraulic radius, S_0 the bed slope, and ρ is the fluid specific mass. From the simulations we calculated mean values of u_* that allow us to estimate possible zones of sediment erosion or deposition caused by turbines interaction with the bed.

2.2. DES-BEM model

In order to simulate turbines and their effects over the environment, we use a Detached-Eddy Simulation (DES) model that solves flow and its turbulence coupled with a Blade Element Momentum (BEM) model. Turbines are represented by a volume V inside the mesh (see Figure 2.3) defined by the rotor center location O, blades radius R, and the rotor depth L, which contains the turbine blades. The turbine forces are calculated from BEM theory and applied to all nodes located within this volume. The model resolution methodology is based on the work of Creech et al. (2015) and was implemented on the DES flow solver by Gajardo et al. (submitted 2018), for more details about the resolution algorithm the reader is referred to Appendix A.

2.2.1. Detached Eddy Simulation

The three-dimensional, incompressible and impermanent flow is solved using the Unsteady Reynolds-averaged Navier-Stokes (URANS) equations for mass and momentum

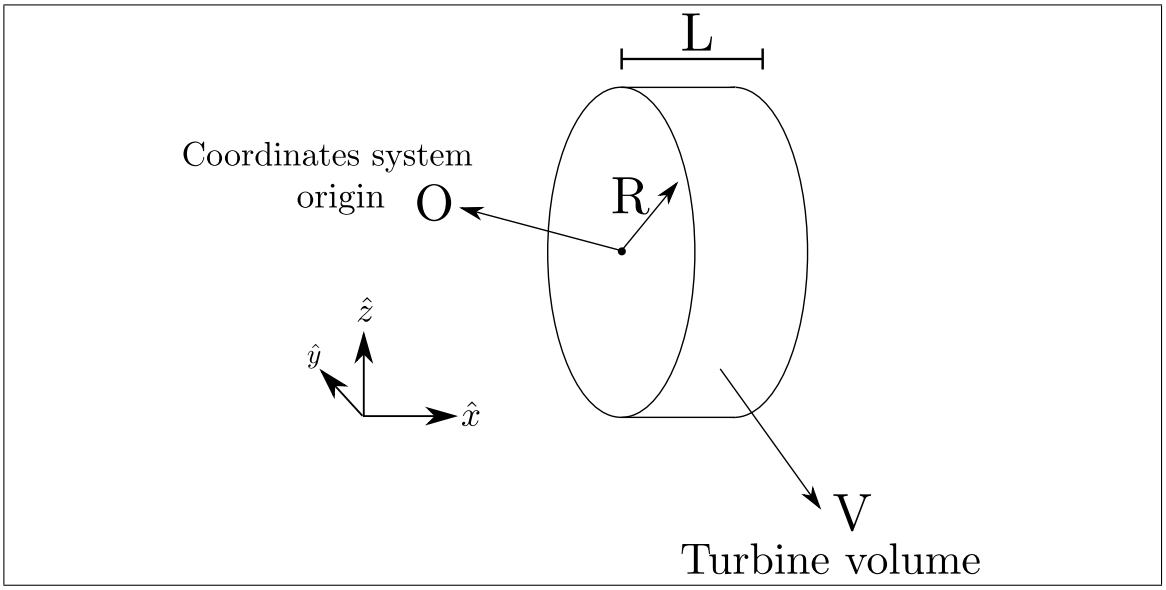

Figure 2.3. Schematic view of cylindral volume V that represents turbines, with local coordinates system origin O, blade radius R and length L. Forces calculated from BEM theory are only applied over nodes inside this volume.

conservation in the DES method developed by Escauriaza & Sotiropoulus (2011c, 2011a, 2011b). Considering the Reynolds decomposition ($U = u + u'$), URANS equations can be written in non-dimensionalized form using tensor notation as:

$$\frac{\partial \tilde{u}_i}{\partial \tilde{x}_i} = 0 \tag{2.2}$$

$$\frac{\partial \tilde{u}_i}{\partial \tilde{t}} + \tilde{u}_j \frac{\partial \tilde{u}_i}{\partial \tilde{x}_j} = -\frac{\partial \tilde{p}}{\partial \tilde{x}_i} + \frac{1}{Re} \frac{\partial^2 \tilde{u}_j}{\partial \tilde{x}_j \partial \tilde{x}_j} - \frac{\partial}{\partial \tilde{x}_j} \langle \tilde{u}_i' \tilde{u}_j' \rangle + \tilde{S}_i \tag{2.3}$$

where Re is the Reynolds number ($Re = \rho U D/\mu$), $\tilde{S}_i$ is the momentum term obtained from BEM approach, which is only considered in the nodes inside volume V. We nondimensionalize the momentum equations, using the water depth H and upstream free stream velocity V as length and velocity scales, respectively.

DES method uses a formulation that combines the Unsteady Reynolds-Averaged Navier-Stokes (URANS) equations with Large Eddy Simulation (LES) equations proposed and

revised by Spalart et al. (1997, 2009). For turbulence uses a one-equation eddy-viscosity model developed by Spalart & Allmaras (P. Spalart & Allmaras, 1992).

The DES model has been used and validated by a several number of studies with different flow conditions and geometries, which validates the model ability for predicting instantaneous flow fields and turbulent structures (Paik, Escauriaza, & Sotiropoulos, 2007; Paik, Sotiropoulos, & Porté-Agel, 2009; Paik et al., 2010; Escauriaza & Sotiropoulos, 2011a, 2011b, 2011c).

2.2.2. Blade Element Momentum

The representation of the real geometry of the blade needs a complex mesh that consumes significant computational resources. An alternative that uses less computational resources for representing the rotor effects over the flow is the BEM method. In this approach, the forces produced by the rotor over the flow (i.e. lift and drag) are determined instantaneously by spatially averaging the local forces acting over rings, which correspond to a radial discretization of a disk with an area equivalent to the rotor cross-section. As seen in Figure 2.4, for a ring of with a radius r, a constant average effect is considered, which depends only on local flow conditions and blade geometry at that specific distance from the origin. The advantage of this method is that the blade characteristics are considered as a source term in the momentum equations, allowing a simpler and better quality mesh to represent the interactions. The disadvantage is that when averaging in time, it is not possible to represent flow characteristics derived from the position of each individual blade (Malki, Masters, Williams, & Nick Croft, 2014).

In our model we used the approach proposed by Creech et al. (2015). Following this approach, Lift (f_L) and Drag (f_D) forces per span unit length are calculated as:

$$f_L = \frac{1}{2}\rho c(r) U_{rel}^2 C_L(\alpha, Re) \tag{2.4}$$

$$f_D = \frac{1}{2}\rho c(r) U_{rel}^2 C_D(\alpha, Re) \tag{2.5}$$

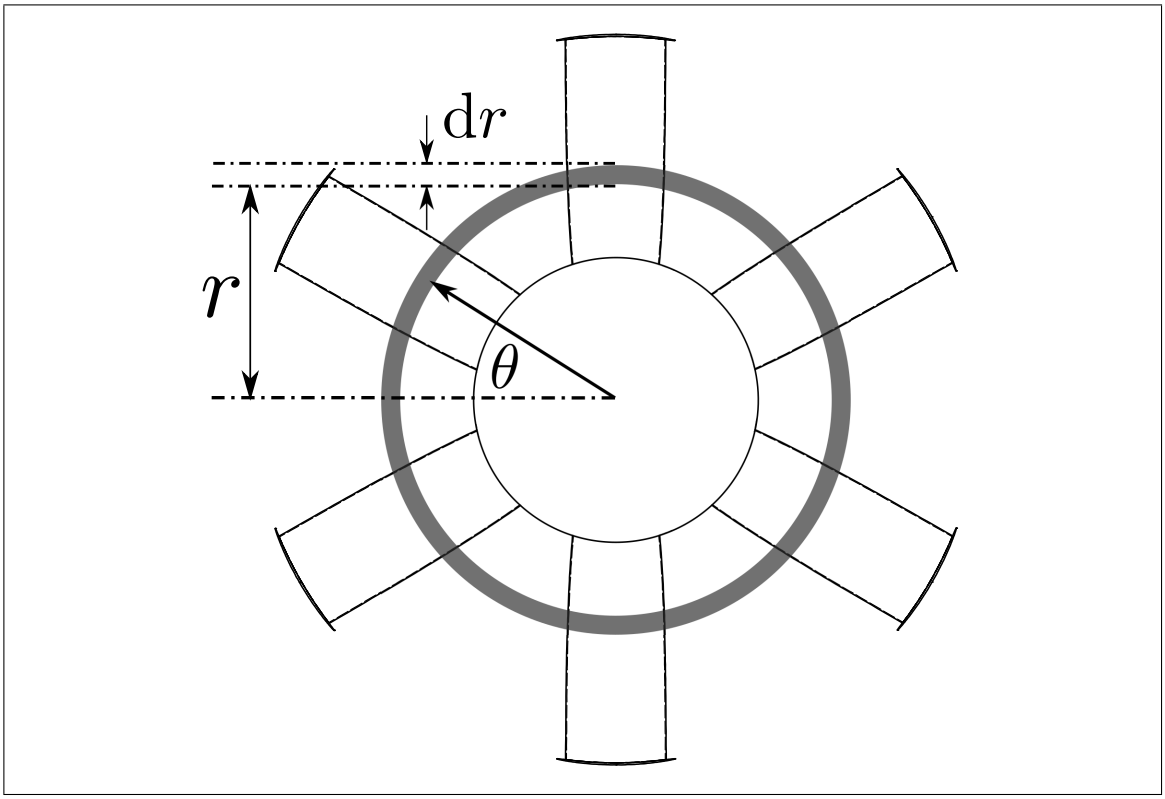

Figure 2.4. Schematic view of turbine rotor. Differential radius width dr is used for rings on BEM approach. Blade characteristics depends on the distance r from the rotor center.

where ρ is fluid density, U_{rel} is the relative speed between the blades and fluid, and $c(r)$ is the blade chord length at a radial distance r from the rotor center. Lift (C_L) and Drag (C_D) coefficients are functions of the blade geometry, the angle of attack α, and the local Reynolds number over the blade. The used values of C_L and C_D were given by the company owner of the turbine for different angles of attack and Reynolds numbers. The BEM method details and how the different terms were calculated can be found in Appendix B.

As the model aims at studying large turbine arrays at low computational costs, the support structure and hub are not represented in the mesh. We opted to represent the nacelle as a region located within the turbine volume V in which all inside nodes has a zero velocity condition on every direction. Even though this option is not the optimal representation of

the nacelle geometry, the results show a good agreement with experimental data as will be discussed in section 3.1.

2.2.3. Grids

The DES computational solver uses structured non-staggered grids and generalized curvilinear coordinates. In both simulations we used rectangular meshes with the same number of nodes in all directions, node distribution only changed between both cases to give a better grid resolution in critical zones where the flow may have abrupt changes. Areas near volume V containing the turbines had a higher density of nodes. The area that contains each turbine has 5 nodes in the longitudinal direction and a dimensionless length corresponding to the width of the area of the rotor that contains the blades. All nodes within the rotor area were equidistributed while outside this zone the spacing varies in such a way as to reach the walls with a distance of $30y^{+}$. An example mesh for the ST case can be seen in Figure 2.5. Table 2.2 shows the most important parameters of both grids.

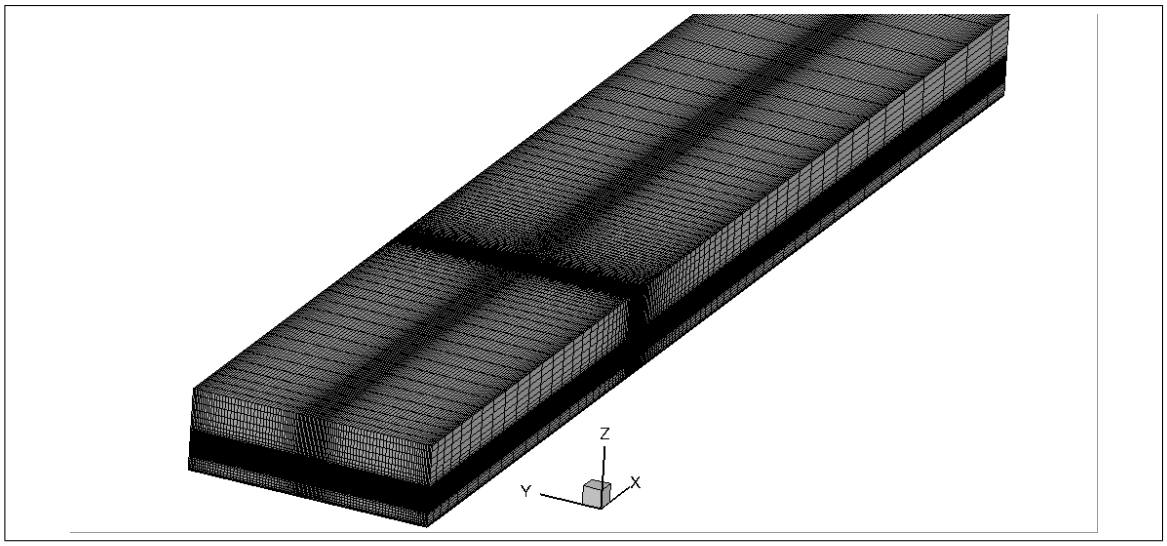

Figure 2.5. Grid used for single turbine (ST) case. For better representation, in every direction only one each three nodes are shown.

Table 2.2. Main grids characteristics used in both cases.

Parameter	Value
$N_x \times N_y \times N_z$	$282 \times 325 \times 101$
Total number of nodes	9,256,650
Number of nodes inside turbine volume	164,125

2.2.4. Boundary conditions

Given that environmental turbulence is an important characteristic of the approaching flow that hydrokinetic turbines faces(Maganga et al., 2010; Mycek, Gaurier, Germain, Pinon, & Rivoalen, 2014a; Blackmore, Myers, & Bahaj, 2016). Our model uses the unsteady inlet condition developed by Smirnov et al. (2001) that is capable of generating synthetic environmental turbulence representative of the flow used in the experimental measurements. The method details can be found in Appendix C.

At the outflow border we used a zero gradient condition. At the bottom of the channel we use a non-slip condition with a sufficient mesh resolution capable of solving the flow viscous sublayer. High resolution at the domain walls is avoided by using a wall function (Kalitzin, Medic, Iaccarino, & Durbin, 2005). For the free surface a rigid-lid or symmetry boundary condition was used. Boundary conditions were the same for both study cases.

3. RESULTS AND DISCUSSION

In this section we present the results for both cases: a single turbine (ST) centered at transverse section, and two turbines (TT) also centered, aligned and separated by 6 turbine diameters. We compare the mean velocity field, the turbulent characteristics of the wake, shear stress, and the scour in the channel bed obtained from measurements and numerical model solution. The turbine performance coefficients (i.e. C_P, C_T), used to estimate turbine response to flow variations, are calculated from DES-BEM model only, while the effects of inflow turbulence over the turbines power output are studied from experimental measurements. All values are shown in dimensionless form using the upstream velocity U_∞ and rotor diameter D for variables as kinematic scales.

3.1. Flow field

A typical way to represent the wake development formed by the turbine, and the recovery of its momentum, is the velocity deficit at the turbine rotor center height within the flume centerline. This variable is defined as:

$$U_{def} = 1 - \frac{U}{U_\infty} \tag{3.1}$$

where U_∞ is the upstream mean velocity facing the turbine, and U is the mean longitudinal flow velocity component at all measured points. Figure 3.1 displays the variation of this variable for the first three downstream diameters counted from the coordinate system origin, for both cases of study.

For the ST case (see Figure 3.1(a)) the values obtained with our DES-BEM model show a difference of 30% and 14.4% respect to experimental values, for the first two points located at 0.5D and 1D, respectively. This difference is due to the inability of the BEM approach to reproduce the shape of the near wake as reported by Masters et al. (2015) and Creech & Früh (2015). The decision of not modeling the turbine hub and support structure is also a factor that inhibits the model to fit better with the experiments in the

near field of the wake. From a distance of 3 diameters downstream from the turbine, values obtained show a good agreement with the experimental measurements. The curve shape is coincident with previously published works (Myers, Bahaj, Germain, & Giles, n.d.; Bahaj, Myers, Rawlinson-Smith, & Thomson, 2012; Stallard, Collings, Feng, & Whelan, 2013b; Gebreslassie et al., 2016). The maximum velocity deficit of 52% is located 2D downstream according to the experimental results. Our model underestimates the velocity deficit at all points, but in the far wake zone the model results improves and get closer to the experiments. This can be observed in the convergence of the experimental and modeled results with the downstream direction.

In the TT case in Figure 3.1(b) the adjustment to experimental data shows larger discrepancies compared to the ST case, this is similar with the wake changes in presence of an upstream obstacle as reported by Chamorro et al. (2015) for a turbine in presence of cylinders upstream. Although the difference in deficit between the origin and 2D is smaller, the curve that describes the wake recovery shows a difference with the experimental values of approximately 5% in average. The model overestimates the deficit after 1D downstream, and the slope of deficit in the far wake zone, despite being similar, shows a convergent trend downstream.

The first three mean longitudinal velocity profiles (U) downstream of the primary turbine, are shown in Figure 3.2 for both cases. The ST case model shows a completely symmetrical wake, as has been reported in different cases for models that uses BEM method (Turnock, Phillips, Banks, & Nicholls-Lee, 2011; Kolekar & Banerjee, 2015; Olczak, Stallard, Feng, & Stansby, 2016; G. Bai, Li, Chang, & Li, 2016). The velocity profile can be approximated as a Gaussian function. In the first diameter downstream the transition between inner and outer areas of rotor shows an abrupt change on the longitudinal velocity, which indicates a low momentum transfer capacity between these two zones at that distance from the turbine. For the next two diameters the transition becomes smoother, showing a greater interaction between the wake and its surrounding flow. The results obtained show a good agreement between the DES-BEM model and experimental results.

However, the model is not able to reproduce the wake asymmetry shown by the experimental results. This asymmetry is due to the hub and support structure interaction with the environmental flow after it passes through the rotor blades.

For cross sections in the TT case a result similar to the ST is obtained. The longitudinal velocity values from the model are similar to the experimental ones, although again the model is not able to reproduce the asymmetry present in the results obtained experimentally. The larger turbulent intensity facing the main turbine, now located in the wake of the secondary turbine, causes the profiles to show less noticeable transitions between the inner and outer rotor areas.

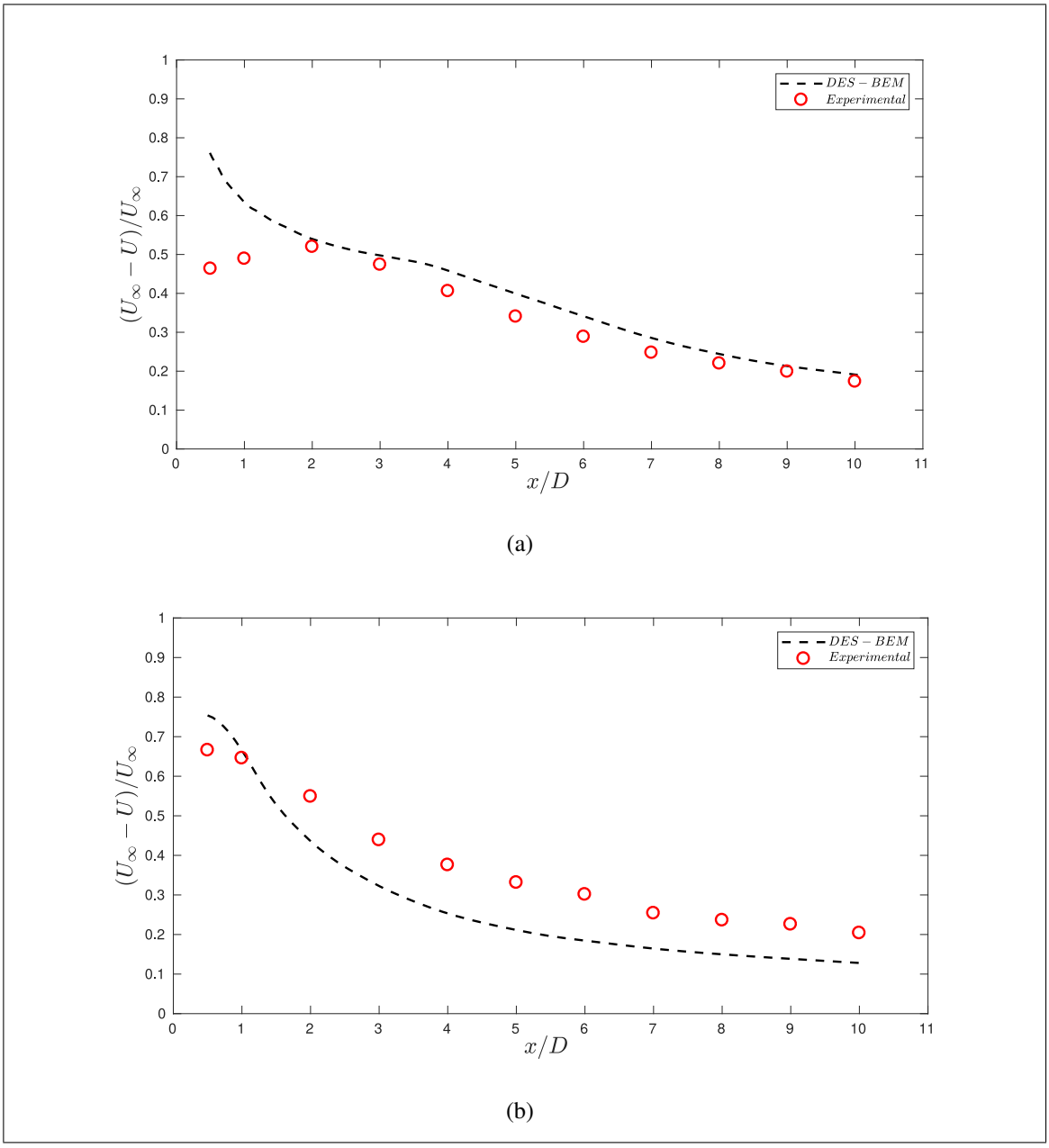

Figure 3.1. Longitudinal mean velocity $\langle U \rangle$ deficit for both study cases normalized by upstream velocity. The ST deficit (a) fits better to experiments than the TT case (b). At $10D$ downstream the wake has recovered an 80% of its mean longitudinal velocity.

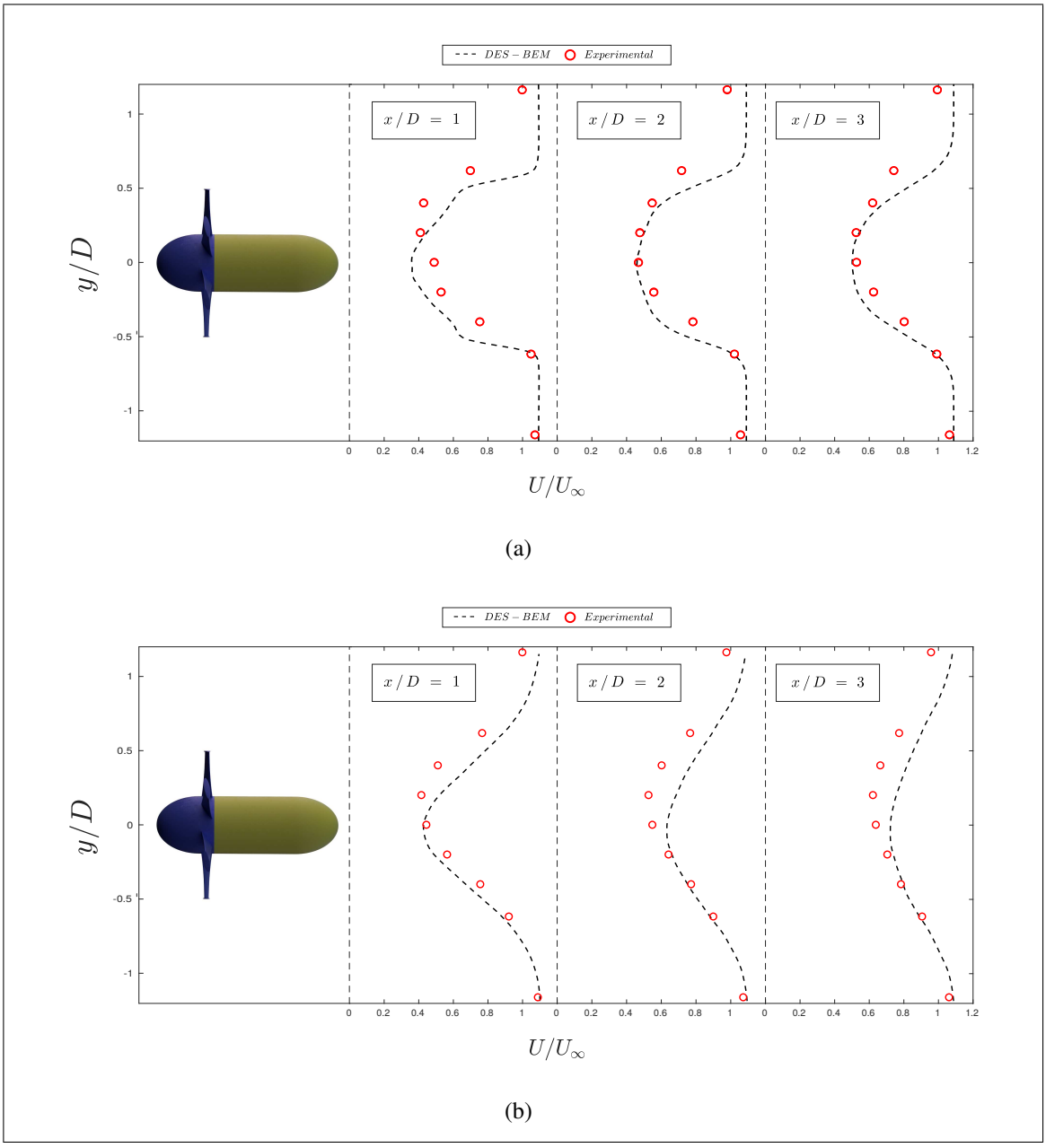

Figure 3.2. Transverse velocity profiles for the first three diameters downstream of the primary turbine for (a) ST and (b) TT cases. DES-BEM model shows agreement with experimental profiles but the model is not capable of representing the asymmetry observed in the measurements.

In Figure 3.3 we can appreciate the first three downstream vertical profiles an influence of the support structure as has been reported previously (Chen, Lin, Lin, & Wang, 2017). As seen in the transverse profiles for the first downstream diameters, the transition between inner and outer rotor regions is abrupt. Within the first diameter, the model results show a symmetry in the wake, further downstream the wake gradually loses symmetry due to the flume bed effect, causing an acceleration of the flow in the upper area of the turbine, and lower velocities near the bottom. Free surface effects can not be seen in the first three diameters, however, when looking at the full velocity field of the channel in Figure 3.4 we can see that the model does not show effects of the free surface in the wake. It has been reported that this is only significant at very high levels of flow blockage (X. Bai, Avital, Munjiza, & Williams, 2014). The DES-BEM model velocities in the near-bed zone show a bad agreement with the experimental results. The model does not represent the turbine support structure, in particular the ballast located at the turbine rear zone, whose axis is coincident with the measurement location. The effect of this structure can be seen to gradually decrease in the first three diameters.

For the TT case we obtained similar results. As shown in Figure 3.2, the larger turbulent intensity in the flow facing the primary turbine, causes a milder transition of the wake between the inner and outer rotor area compared to the ST case. Also, the influence of the support structure rear ballast on the longitudinal velocity near the flume bed becomes smaller. The vertical profiles are more homogeneous and the rotor presence has a less significant impact.

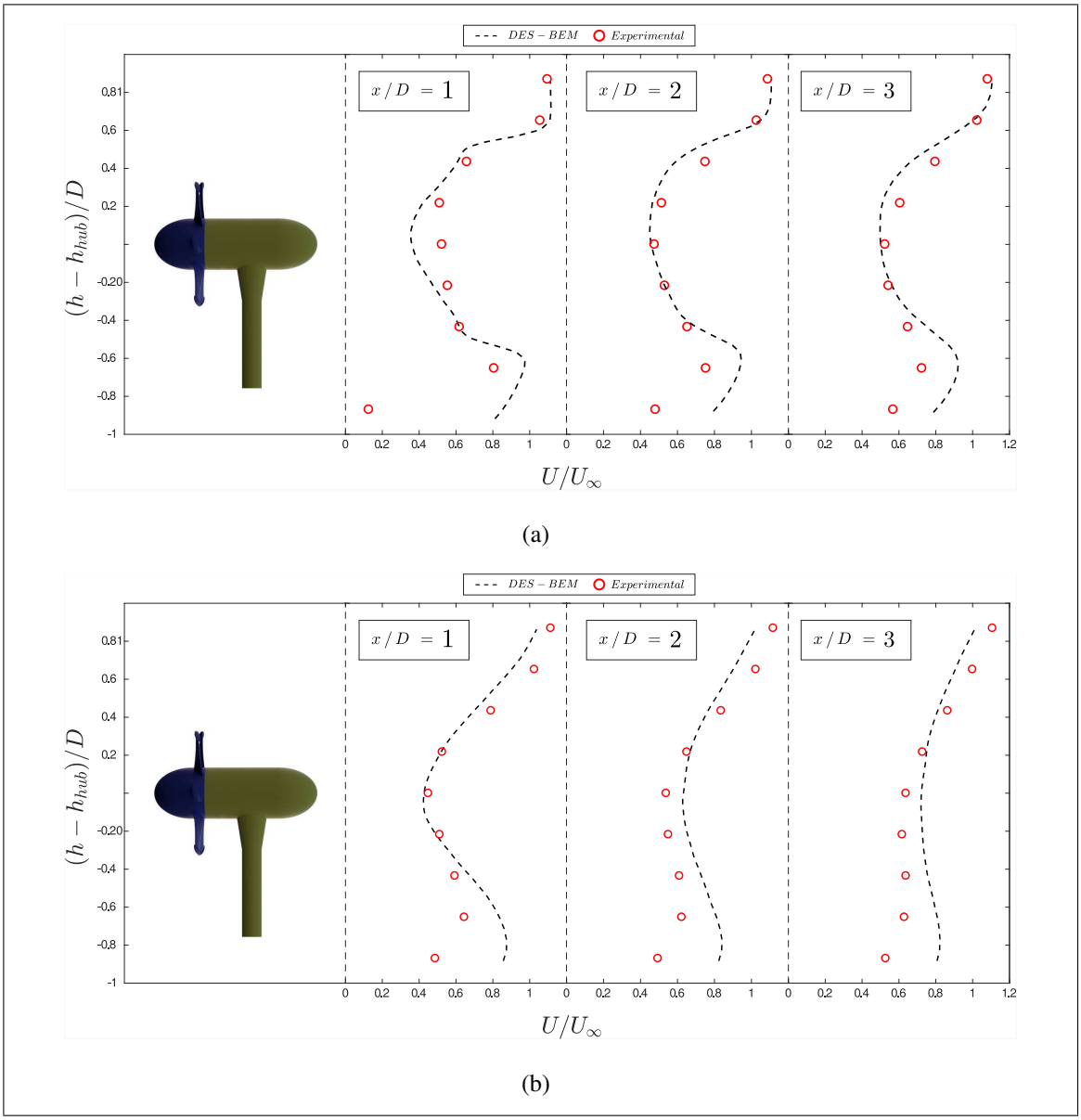

Figure 3.3. Vertical longitudinal velocity profiles for ST (a) and TT (b) cases.

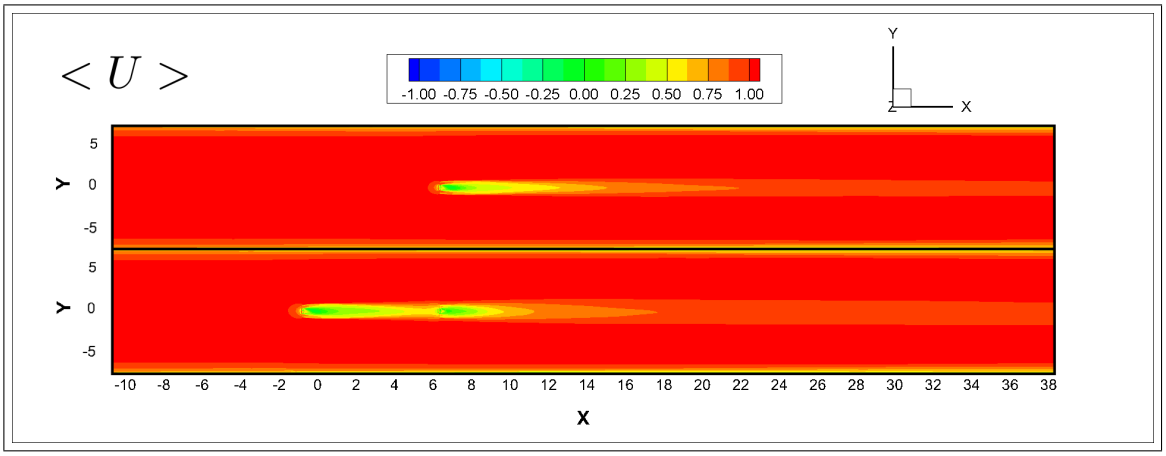

Figure 3.4. XZ-plane of average longitudinal velocity $\langle U \rangle$ for ST and TT cases at rotor center height. For better representation Y-axis is amplified.

In order to visualize the dynamics of the three-dimensional coherent structures, we employ the so-called q criterion proposed by Hunt et al. (1988), where q is defined as:

$$q = \frac{1}{2}\left(\|\Omega\|^2 - \|S\|^2\right) \tag{3.2}$$

where $\|\cdot\|$ is the Euclidean matrix norm and Ω and S are the symmetric and antisymmetric parts derived from the velocity gradient. Regions where vorticity is greater than the rate-of-strain magnitude (i.e. $q > 0$) are occupied by vortical structures (Hunt et al., 1988).

Figure 3.5 shows instantaneous q iso-surfaces in the wakes for the cases of a ST and TT, capturing the interaction of the devices and the differences. Due to the BEM approach approximations, our model fails to represent the effects of each blade tip on the flow. The rotor is modeled in such way that generates periodic vortices of annular form on the flow coming from all the averaged blade tips, which propagate downstream and interact with the ambient flow surrounding the turbine, favoring the momentum exchange and making the wake expand. We can see the nacelle represented as a zone of zero velocity and high pressure in the rotor center, from where periodic rotational vortices are also generated and interact with the annular vortices produced by the blade tips.

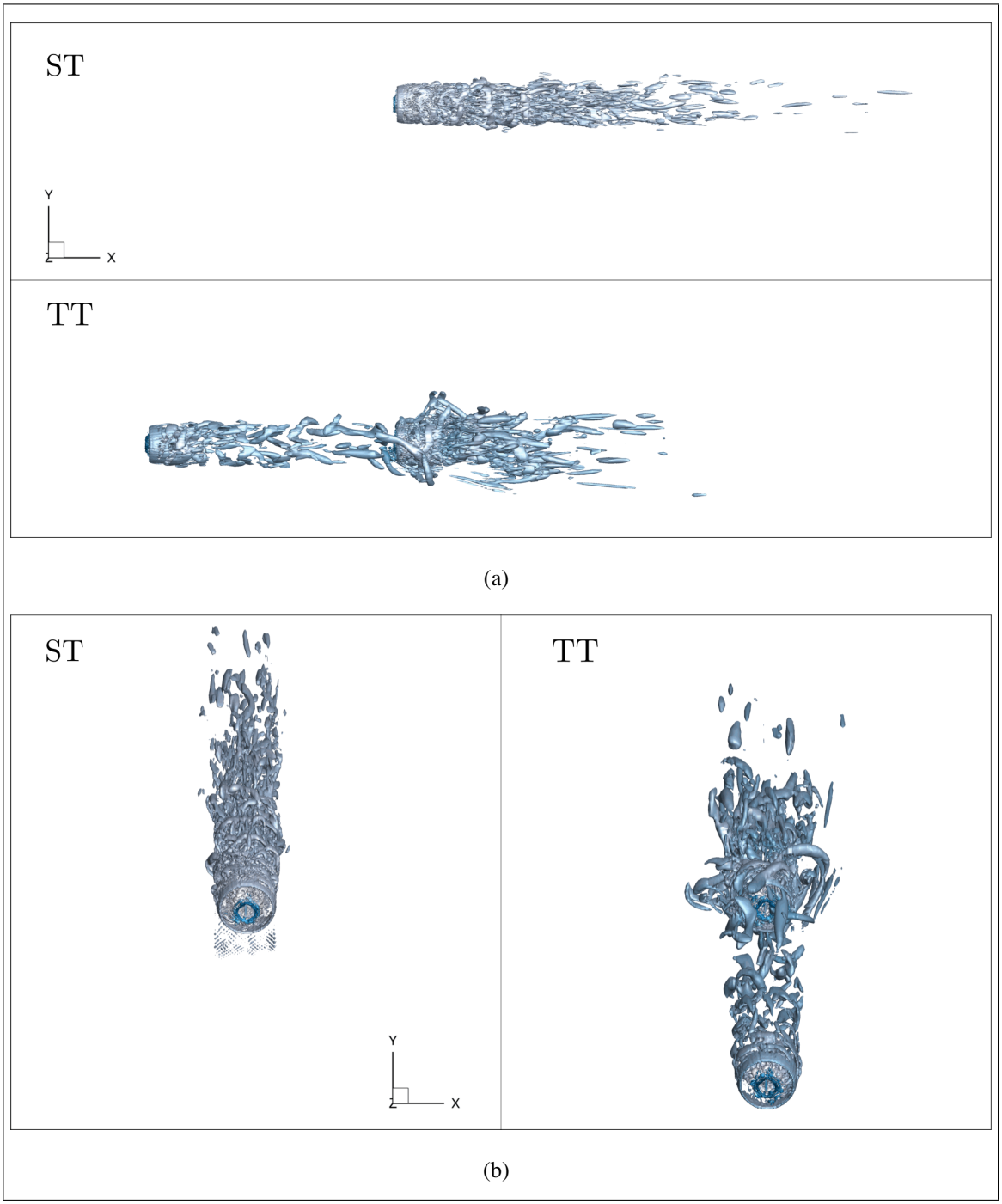

Figure 3.5. Instantaneous q-iso surfaces from two different views. Both cases shows the annular vortex produced by the averaged blade tips, and the high pressure point at the nacelle area. Wake vortical structures are shorter for the TT case due to the greater turbulent intensity that faces the primary turbine in that case.

Comparing the instantaneous view of the coherent structures produced by the downstream turbine in both cases studied, we see a shorter wake in the TT case that is coincident with the mean velocity field of Figure 3.4. As reported by Blackmore et al. (2016), the wake length is smaller when there is a structure that generates greater turbulent intensity upstream of the turbine, since it favors the mixing process and makes the longitudinal velocity to recover faster.

The results presented in this section for mean and instantaneous flow help us understand the turbine-flow interaction and how wakes develop and merge downstream from turbines. Our model by itself is not capable of reproduce the wake asymmetry and other flow characteristics due to BEM approach simplifications. Scale model experiments performed at laboratory are good complementary tools for our DES-BEM model as can be seen in our results. Both are necessary instruments to fully understand the wake dynamics of turbine arrays, and be able to apply this results for modeling bigger farms of devices in a near future. Besides, it is important to consider the purpose behind using this models for predicting flow-turbine interaction. Since in arrays the distance between turbines is larger than the near wake zone, this approach with BEM should work for estimate enough flow parameters for turbine developers.

3.2. Turbine performance

To characterize the turbine performance we can use the power C_P and thrust coefficients C_T to compare the performance of devices installed in different locations in the channel. The power coefficient is defined as the ratio between power extracted by the turbine blades, and the theoretical maximum power available in the flow facing the turbine. This non-dimensional variable is defined as follows:

$$C_P = \frac{P}{0.5\rho U_\infty^3 A_d} \tag{3.3}$$

where U_∞ is the free stream velocity upstream of the devices, A_d is the frontal area swept by the blades, and P is the power obtained by integrating the contribution of every node

inside the turbine volume V:

$$P = \int_V \Omega' \left(r F_{azim} \right) dV \tag{3.4}$$

where Ω' is the turbine rotational velocity and F_{azim} is the azimuthal component of the force acting on each blade. For further details of this variables the reader is referred to BEM method explanation in Appendix B.

The thrust coefficient is defined as the ratio between the axial force acting over the turbine in flow direction, and the mean turbulent kinetic energy (TKE) available in the flow facing the turbines. It is calculated as:

$$C_T = \frac{T}{0.5 \rho U_\infty^2 A_d} \tag{3.5}$$

where the total thrust on the turbine, T, is obtained in a similar way to P:

$$T = \int_V \left(F_x \right) dV \tag{3.6}$$

where F_x is the longitudinal force component acting on the turbine blades.

In Figure 3.6 we can see box plots for C_P and C_T obtained from the time series of the DES-BEM model. The power coefficient for the ST case is approximately $C_P = 0.28$, meanwhile for the TT case it is reduced almost by half ($C_P = 0.15$). This decay in turbine performance can be seen as an effect of the presence of the secondary turbine upstream, which causes a reduction in 20% in the longitudinal velocity facing the primary turbine, and as a consequence of the proximity between both devices ($6D$), which does not allow the wake to recover its velocity completely.

In order to characterize the turbine performance variability we calculated the Coefficient of Variation C_V, a standardized measure of data series dispersion calculated as the ratio between standard deviation σ to the mean μ of a time series. For the TT case C_V of C_P is 5 times higher compared with the ST case. On the other hand, the thrust coefficient C_T is also an indicator of turbine performance typically used, and it indicates the thrust

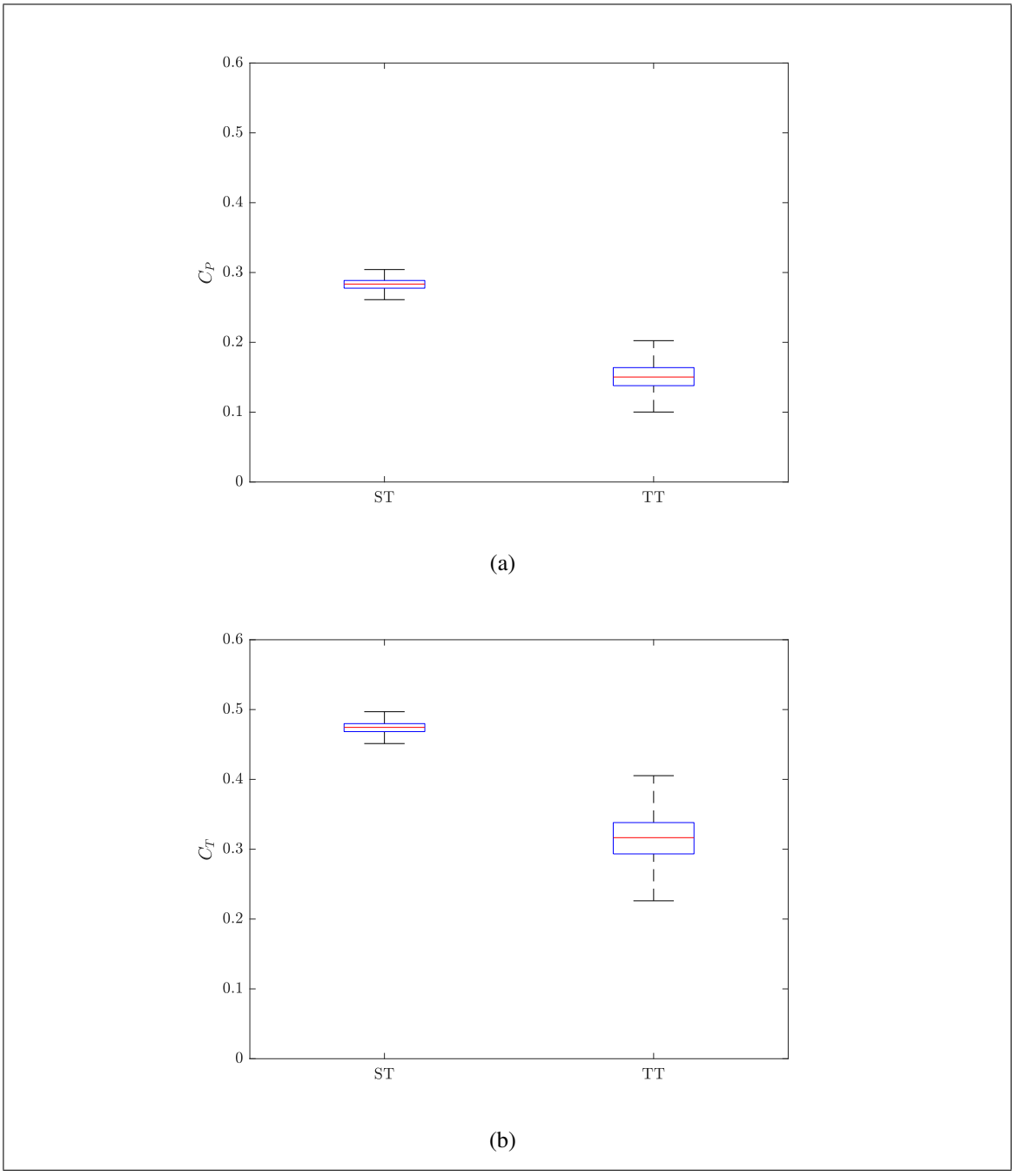

Figure 3.6. Thrust (C_T) and Power (C_P) coefficients for both studied cases. Between the ST case and the TT the average value of the coefficients varies by 46 % and 33 % for C_P and C_T, respectively. The coefficient of variability (C_V) of C_P increases 5 times between both cases, while for C_T the value is 6 times.

force that devices will experience under operation. From our simulations we obtained for C_T similar results to C_P. For the ST case, the mean C_T obtained value from simulations is 0.47 which decrease to 0.32 for the TT case, showing a 33% variation. The Coefficient of Variation C_V increased almost 6 times between our two study cases.

The mean decrease in both coefficients and the variability increase is an expected result. The greater turbulence level facing the primary turbine when located into the wake of another device causes more variability for both C_P and C_T. This variability is an important result that must be taken into account by turbine designers when planning different farm layouts of MHK turbines. C_P is important for planning the connection of these arrays into the electric grid of any country since it provides an estimate of the energy that the device can extract from the flow, meanwhile C_T is crucial for designers to predict possible blade material fatigue that may affect the lifespan of turbines. In our work we did not performed measurements for different longitudinal and spanwise spacing between turbines or arrays, so a more methodical approach can be followed, controlling such variables and then examining how they influence overall turbine performance and wake development.

The spectrum of instantaneous voltage measurements is an indicator of the turbine operating characteristics. Even though the voltage obtained in our experiments is not properly scaled to prototype, voltage spectrum fluctuations are used as a proxy of how this devices will respond to flows like this on similar conditions (Hill et al., 2016). For our experiments we calculated the voltage spectrum of the measurements obtained from the primary turbine for both cases, as seen in Figure 3.7. The first peak of both curves is coincident with the correspondent turbine frequency (f_{ST} , f_{TT}), while the following are their resonant peaks. At low frequencies there is a difference between both spectra explained by the influence of surrounding flow while for higher frequencies this effects are not perceived acting over the turbine performance (Chamorro et al., 2013)

In order to characterize the turbine influence over the flow we calculated the longitudinal velocity spectra showed in Figure 3.8 for one point located upstream both turbines and the second one positioned $10D$ downstream from the primary turbine, both at hub

height within flume centerline. From our results we can observe that in lower frequencies there is a change between the upstream and downstream spectra, which indicates that low frequencies are affected by the turbine presence in the same way that we observed in the voltage spectrum. For both cases, areas under the plot are bigger for the downstream point, which indicates a greater performance variability just as expected.

Thrust and power coefficients obtained from our model are estimations of turbines performance. The incoming flow turbulent intensity produces evident effects over both parameters. For larger turbulent intensity there is a decrease of C_P and C_T, and an increase in variability. The influence of flow turbulent intensity over turbine performance is also reflected over voltage and velocity spectra. The low frequency variation observed in our results and reported by different authors for other devices is evidence that must be taken into account by turbine developers to predict a possible blade fatigue damage or power fluctuations.

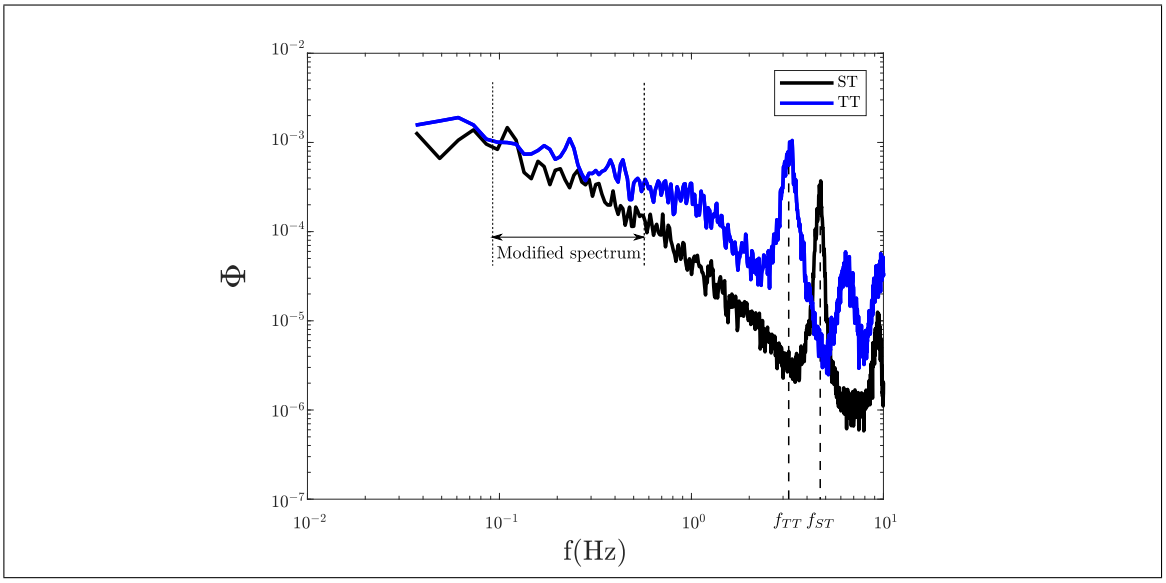

Figure 3.7. Voltage spectrum for both study cases. First peaks indicate primary turbine rotational frequency for each case. At lower frequencies surrounding flow effects are perceived.

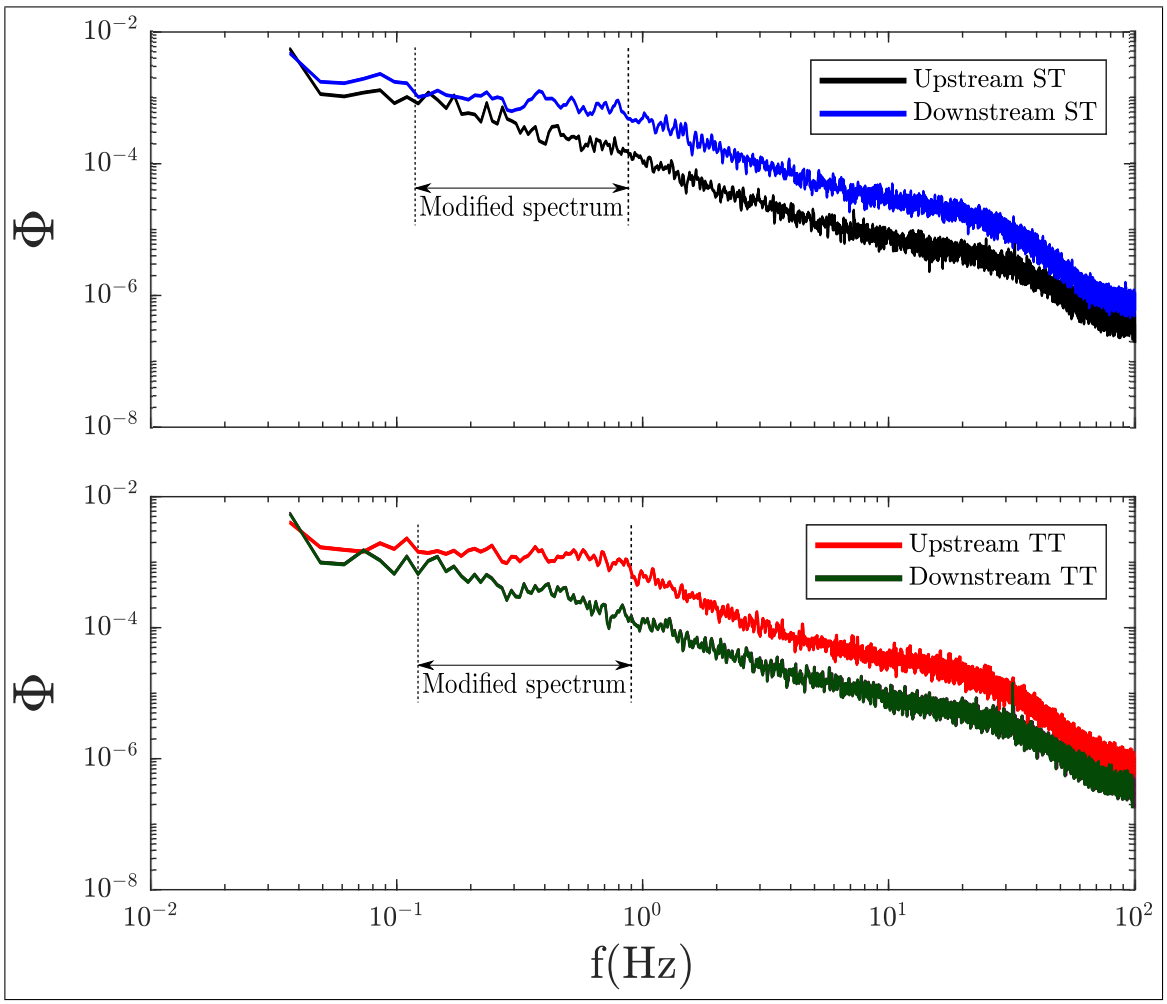

Figure 3.8. Velocity spectrum upstream and downstream of primary turbine for ST (a) and TT (b) cases. Surrounding flow effects are perceived in same frequency range of voltage spectrum.

3.3. Turbine-Bathymetry interaction

Turbines interaction with flume bed generates scouring and deposition of sediment even in clear-water conditions. In Figure 3.9 (a) we show the bed elevation changes after the experiments, which were conducted in the same conditions and during the same period of time, with respect to the original bed level registered before measurements. Just as expected, the support structure generates scouring zones right next to the ballasts meanwhile downstream of the turbine there are deposition zones produced by the rear ballast and the wake longitudinal velocity deficit. This deposition is less notorious downstream of the primary turbine for the TT case due to the lower velocity deficit between upstream and downstream this device (see Figure 3.1). From 4 to 6 diameters downstream, there is a deposition zone over the left bank, which is coincident with the asymmetry observed in the transverse longitudinal velocity profile of Figure 3.2. This phenomena was not replicated by our DES-BEM model simulations, thus we can consider this effect to be caused by the turbine elements that are not being represented in our model, i.e. hub and support structure.

If we compare the primary turbine wake on the ST case and secondary turbine wake for the TT case, both facing an undisturbed flow with longitudinal velocity U_∞, we can appreciate a difference between the maximum deposition height, as can be appreciate in Figure 3.10. The cause of this difference is not clear yet, even though we can state two possible reasons: (1) the presence of another turbine located downstream produces an effect over the flow dynamics of the upstream turbine wake, and (2) the TSR difference between both turbines (3.65 for ST and 2.0 for TT) generates lower flow-bathymetry interactions due to its different wake dynamics. This effect can be also noted on the model results as the u_* is lower for the TT secondary turbine in comparison with the ST primary device. In order to clarify which option is the main cause, further experiments and simulations with our model or other must be performed in future research.

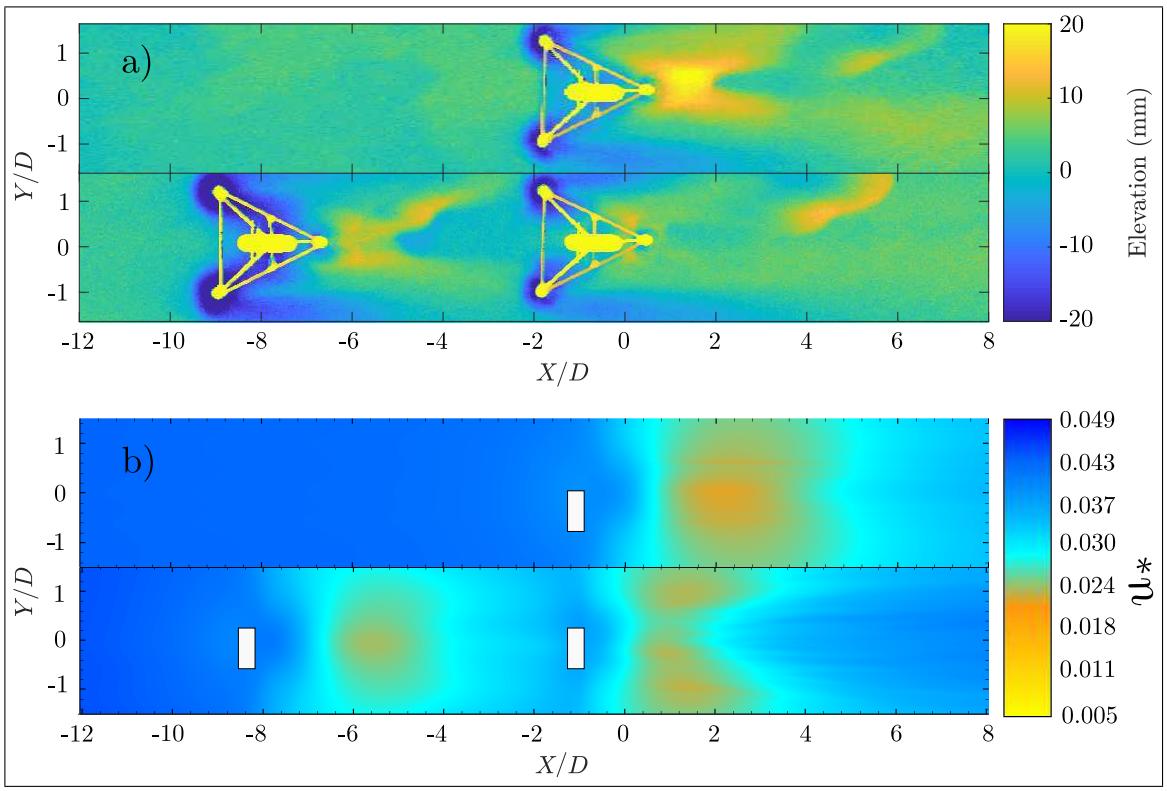

Figure 3.9. (a) Experimental elevation after experiments and (b) average shear stress calculated from DES-BEM model. DES-BEM model results show a similar low-shear zone after turbines which is coincident with experimental measurements.

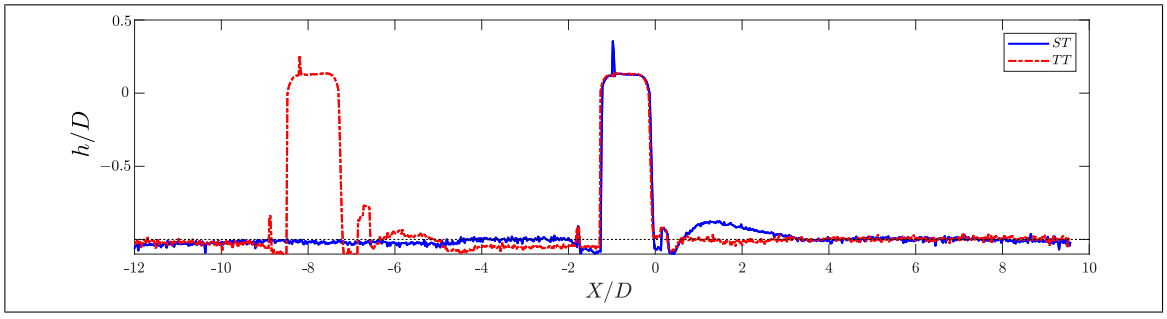

Figure 3.10. Final centerline bed elevation after experiments for ST and TT cases. Vertical axis scale is distorted for better representation.

The shear stress, represented by the u_* parameter in Figure 3.9 (b), works as an indicator of zones where scouring or deposition are favored. In the ST simulation results we observe a low u_* zone between 1D and 4D downstream the primary turbine, which is coincident with experimental results as the location of this deposition zone is the same. Nevertheless, the shape of this zone differs from measurements as the V-shape deposition zone observed in the experiments behind all turbines it is not present in our simulation results due to the absence of the support structure in our model, specifically the rear ballast. For TT case between 0D and 3D downstream the results are similar, there is a low shear zone also coincident with experimental results that presents a similar shape to the one seen in the experimental measurements.

In Figure 3.11 transverse elevation profiles for 1D up to 6D downstream the primary turbine are shown. As commented from Figure 3.9, within the first 2 diameters the bed elevation is greater for the ST case. For the ST profile at 2D a depression zone can be observed slightly to the left from the center. This asymmetry is coincident with the maximum velocity deficit showed in Figure 3.2. On the right side of the flume, and up to 4D downstream, for both cases there is a scour zone produced by a flow acceleration. For the first 3D there is no significant variations of bed elevation for the TT case, while for 5D and 6D a deposition zone is present on the profiles left side. After 6D downstream there is no signal of large sediment structures caused by flow-bed interactions induced by turbines.

The way these devices interact with the environment either alone or in arrays is still a major challenge for turbine designers. The turbine effects over flow depends on the device geometry and its operational parameters. The results obtained by our model suggest that some main characteristics of this interaction can be represented by DES-BEM model, while the bed elevation asymmetry in the wake indicates a necessity of considering support structure and hub into our model. This discussion must be continued on future research either through numerical simulations or experiments, in order to really understand the limits and scope of each one of this analysis methods and to prevent local environmental impacts produced by MHK devices.

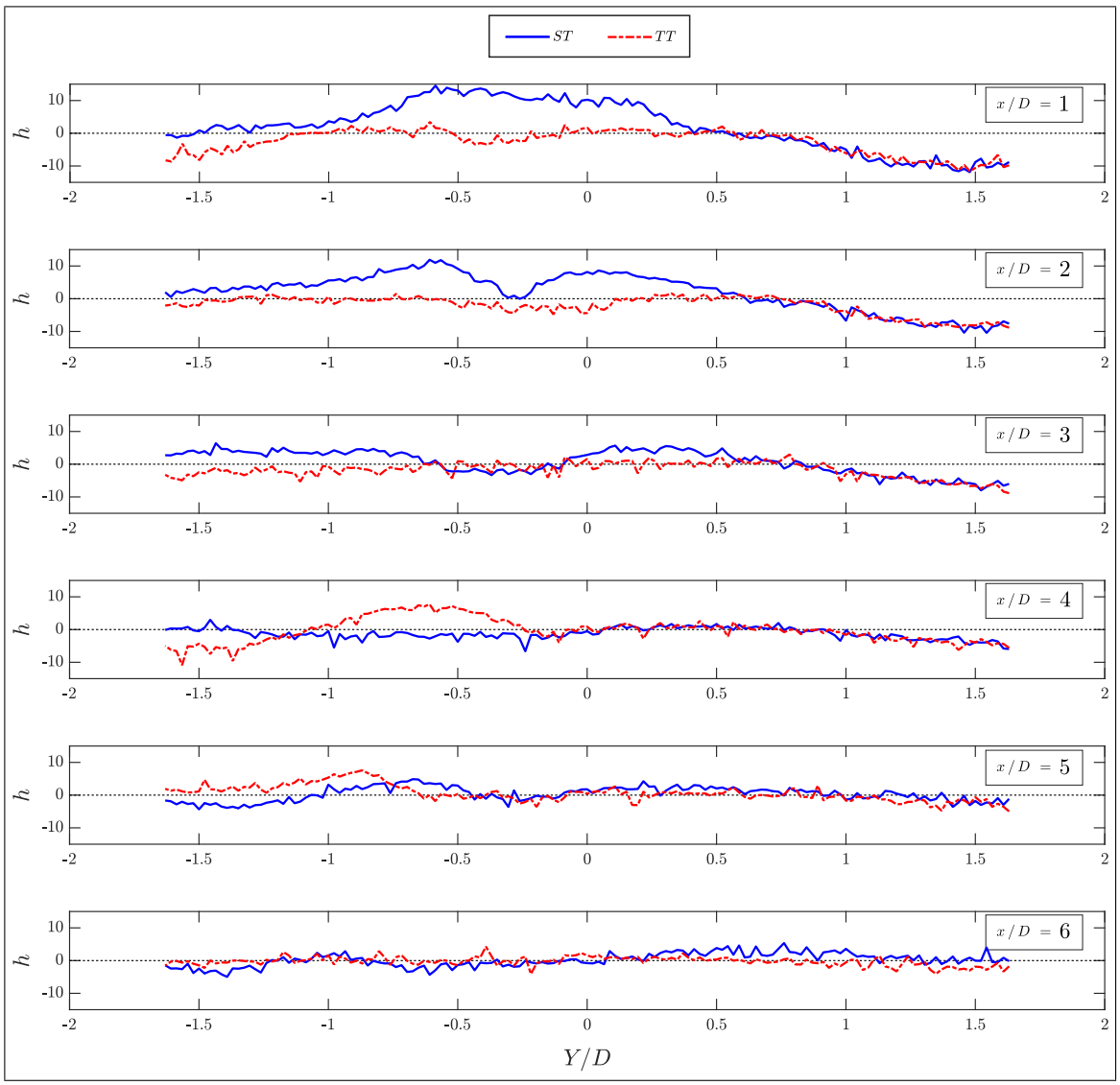

Figure 3.11. Transverse bed elevation profiles up to $6D$ downstream of primary turbine for ST and TT cases.

4. CONCLUSIONS AND FUTURE WORK

In this work we studied the D10 Sabella turbine using laboratory experiments and numerical simulations to characterize the flow dynamics in the wake produced by the turbine, the power performance, and the turbine-bathymetry interaction for two different cases in clear water conditions: a single turbine, and two turbines aligned and separated by six diameters. Simulations were performed using a DES-BEM model implemented by Gajardo et al. (submitted 2018). The DES flow solver used in this model is based on the work done by Escauriaza & Sotiropoulus (2011b), while the BEM tidal turbine representation approach is based on the work done by Creech et al. (2015). The model incorporates ambient turbulence using the Random Flow Generator technique proposed by Smirnov et al. (2001) into the inlet flow boundary condition.

The comparison of the DES-BEM simulation results with the experimental measured data showed that our model is capable of reproducing the mean values of longitudinal velocity. The region where worst results were appreciated was in the near wake zone, where the absence of the hub, the support structure, and the nacelle representation into our model is the main factor. Besides, the velocity profile asymmetry reported in the experiments, as well as tip vortices and wake meandering, were not present in the numerical results due to BEM approach simplifications. Despite these differences, the DES-BEM model is a good tool for predicting averaged wake magnitudes in comparison with more complex models and at lower computational cost, which makes it a powerful modeling approach for larger arrays. This would be unfeasible to do with more geometry-accurate models. Furthermore, we think these differences can be neglected by turbine designers considering that usually turbines are located in arrays with such separation that downstream devices are never into the near wake zone.

The flow complexity that faces the turbine when is located in the wake of another device is proportional to the turbulent intensity (Maganga et al., 2010; Blackmore, Batten, & Bahaj, 2014). As reported by several authors, the variability of the performance of

turbines is closely related to this parameter. The turbine rotational frequency dependence on the incoming flow characteristics is evident in the voltage spectra for both cases. The magnitude of this variability has to be considered by turbine developers when selecting a flow solver. This work shows that a DES solver coupled with simpler turbine approaches like BEM, offers improved results compared to models with higher geometrical resolutions but lower flow details. This approach has proven their capability of reproduce mean values and fluctuations of flow velocity using less computational resources.

The way this devices affects the environment depends on the turbine-flow-bathymetry interaction. Our results indicate a relation between scouring and deposition of sediments with the dynamics of the wake. The asymmetry present in our results was reflected in how the bathymetry evolves in the wake zone. As wake characteristics depends on different parameters such as turbine hub, support structure, and TSR, it is important to study these parameters separately to identify how they can affect the sediment transport dynamics.

Laboratory experiments coupled with numerical simulations are a necessary combination of tools to reach an understanding of how MHK turbines work. A DES flow solver is capable of reproducing turbulent characteristics of the velocity field when a simple turbine representation like BEM is implemented, and has shown a better agreement with experimental results than other models with more accurate blade geometry representation that use simpler flow solvers (Gajardo et al., submitted 2018). Laboratory experiments are necessary to validate numerical models and mostly to understand their flaws, in a way that the complementary nature of this two tools is unquestionable.

Future work will include characterization of different turbine arrays aligned or staggered, controlling lateral and longitudinal separation, setting TSR to those indicated as design parameter, and using different turbine-flow orientation. Also, other tools like Particle Image Velocimeter (PIV) can be employed to get synoptical views of the velocity field to analyze the different vortical structures produced in the wake. Mesh refinement studies and its effect over the C_P and C_T estimations are not considered here. In addition, BEM coefficient modifications to include tip effects or other flow-turbine interactions are

still missing. However, all this analysis are possible improvements for the model in future work. Finally, the implementation of other turbine representation approaches, such as Actuator Lines (AL) into the DES flow solver is another alternative that could be considered for future performance analysis.

REFERENCES

Abutunis, A., Hussein, R., & Chandrashekhara, K. (2018). A Neural Network Approach to Enhance Blade Element Momentum Theory Performance for Horizontal Axis Hydrokinetic Turbine Application. *Renewable Energy*. Retrieved from https://linkinghub.elsevier.com/retrieve/pii/S0960148118311807 doi: 10.1016/j.renene.2018.09.105

Ahmadi, M. H. (2018). Influence of upstream turbulence on the wake characteristics of a tidal stream turbine. *Renewable Energy*, *132*, 989–997. Retrieved from https://linkinghub.elsevier.com/retrieve/pii/S096014811831005X doi: 10.1016/j.renene.2018.08.055

Allsop, S., Peyrard, C., Thies, P. R., Boulougouris, E., & Harrison, G. P. (2017). Hydrodynamic analysis of a ducted, open centre tidal stream turbine using blade element momentum theory. *Ocean Engineering*, *141*(July), 531–542. Retrieved from http://dx.doi.org/10.1016/j.oceaneng.2017.06.040 doi: 10.1016/j.oceaneng.2017.06.040

Apsley, D. D., Stallard, T., & Stansby, P. K. (2018). Actuator-line CFD modelling of tidal-stream turbines in arrays. *Journal of Ocean Engineering and Marine Energy*. Retrieved from http://link.springer.com/10.1007/s40722-018-0120-3 doi: 10.1007/s40722-018-0120-3

Bahaj, A. S., Myers, L. E., Rawlinson-Smith, R. I., & Thomson, M. (2012). The Effect of Boundary Proximity Upon the Wake Structure of Horizontal Axis Marine Current Turbines. *Journal of Offshore Mechanics and Arctic Engineering*, *134*(2), 021104. Retrieved from http://offshoremechanics.asmedigitalcollection.asme.org/article.aspx?articleid=1457736 doi: 10.1115/1.4004523

Bai, G., Li, W., Chang, H., & Li, G. (2016). The effect of tidal current directions on

the optimal design and hydrodynamic performance of a three-turbine system. *Renewable Energy*, *94*, 48–54. Retrieved from http://dx.doi.org/10.1016/j.renene.2016.03.009 doi: 10.1016/j.renene.2016.03.009

Bai, X., Avital, E. J., Munjiza, A., & Williams, J. J. (2014). Numerical simulation of a marine current turbine in free surface flow. *Renewable Energy*, *63*, 715–723. Retrieved from http://dx.doi.org/10.1016/j.renene.2013.09.042 doi: 10.1016/j.renene.2013.09.042

Batten, W. M. J., Harrison, M. E., & Bahaj, A. S. (2013, jan). Accuracy of the actuator disc-RANS approach for predicting the performance and wake of tidal turbines. *Philosophical Transactions of the Royal Society A: Mathematical, Physical and Engineering Sciences*, *371*(1985), 20120293. Retrieved from http://www.ncbi.nlm.nih.gov/pubmed/23319711http://rsta.royalsocietypublishing.org/cgi/doi/10.1098/rsta.2012.0293 doi: 10.1098/rsta.2012.0293

Blackmore, T., Batten, W. M., & Bahaj, A. S. (2014). Influence of turbulence on the wake of a marine current turbine simulator. *Proceedings of the Royal Society A: Mathematical, Physical and Engineering Sciences*, *470*(2170). doi: 10.1098/rspa.2014.0331

Blackmore, T., Myers, L. E., & Bahaj, A. S. (2016). Effects of turbulence on tidal turbines: Implications to performance, blade loads, and condition monitoring. *International Journal of Marine Energy*, *14*, 1–26. Retrieved from http://dx.doi.org/10.1016/j.ijome.2016.04.017 doi: 10.1016/j.ijome.2016.04.017

Bowman, J., Bhushan, S., Thompson, D. S., O'Doherty, D., O'Doherty, T., & Mason-Jones, A. (2018). A Physics-Based Actuator Disk Model for Hydrokinetic Turbines. *2018 Fluid Dynamics Conference*, 1–20. Retrieved from https://arc.aiaa.org/doi/10.2514/6.2018-3227 doi: 10.2514/6.2018-3227

Burton, T., Jenkins, N., Sharpe, D., & Bossanyi, E. (2011). *Wind energy handbook*. John Wiley & Sons.

Chamorro, L. P., Hill, C., Morton, S., Ellis, C., Arndt, R. E. a., & Sotiropoulos, F. (2013). On the interaction between a turbulent open channel flow and an axial-flow turbine. *Journal of Fluid Mechanics*, *716*, 658–670. doi: 10.1017/jfm.2012.571

Chamorro, L. P., Hill, C., Neary, V. S., Gunawan, B., Arndt, R. E., & Sotiropoulos, F. (2015). *Effects of energetic coherent motions on the power and wake of an axial-flow turbine* (Vol. 27) (No. 5). doi: 10.1063/1.4921264

Chen, Y., Lin, B., Lin, J., & Wang, S. (2017, jun). Experimental study of wake structure behind a horizontal axis tidal stream turbine. *Applied Energy*, *196*, 82–96. Retrieved from http://dx.doi.org/10.1016/j.apenergy.2017.03.126http://linkinghub.elsevier.com/retrieve/pii/S0306261917303720 doi: 10.1016/j.apenergy.2017.03.126

Creech, A., Früh, W. G., & Maguire, A. E. (2015). Simulations of an Offshore Wind Farm Using Large-Eddy Simulation and a Torque-Controlled Actuator Disc Model. *Surveys in Geophysics*, *36*(3), 427–481. doi: 10.1007/s10712-015-9313-7

Edmunds, M., Williams, A. J., Masters, I., & Croft, T. N. (2017). An enhanced disk averaged CFD model for the simulation of horizontal axis tidal turbines. *Renewable Energy*, *101*, 67–81. Retrieved from http://dx.doi.org/10.1016/j.renene.2016.08.007 doi: 10.1016/j.renene.2016.08.007

Escauriaza, C., & Sotiropoulos, F. (2011a). Initial stages of erosion and bed form development in a turbulent flow around a cylindrical pier. *Journal of Geophysical Research: Earth Surface*, *116*(3), 1–24. doi: 10.1029/2010JF001749

Escauriaza, C., & Sotiropoulos, F. (2011b, jan). Lagrangian model of bed-load transport in turbulent junction flows. *Journal of Fluid Mechanics*, *666*, 36–76. Retrieved from http://www.journals.cambridge.org/abstract{_}S0022112010004192 doi: 10.1017/S0022112010004192

Escauriaza, C., & Sotiropoulos, F. (2011c). *Reynolds number effects on the coherent dynamics of the turbulent horseshoe vortex system* (Vol. 86) (No. 2). doi: 10.1007/s10494-010-9315-y

Gajardo, D., Escauriaza, C., & Ingram, D. (submitted 2018). Investigation on tidal

arrays with a coupled DES-BEM model. *Renewable Energy*.

Gebreslassie, M. G., Sanchez, S. O., Tabor, G. R., Belmont, M. R., Bruce, T., Payne, G. S., & Moon, I. (2016). Experimental and CFD analysis of the wake characteristics of tidal turbines. *International Journal of Marine Energy*, *16*, 209–219. Retrieved from http://dx.doi.org/10.1016/j.ijome.2016.07.001 doi: 10.1016/j.ijome.2016.07.001

Hill, C., Musa, M., Chamorro, L. P., Ellis, C., & Guala, M. (2014). Local Scour around a Model Hydrokinetic Turbine in an Erodible Channel. *Journal of Hydraulic Engineering*, *140*(8), 04014037. Retrieved from http://ascelibrary.org/doi/10.1061/{%}28ASCE{%}29HY.1943-7900.0000900 doi: 10.1061/(ASCE)HY.1943-7900.0000900

Hill, C., Musa, M., & Guala, M. (2016). Interaction between instream axial flow hydrokinetic turbines and uni-directional flow bedforms. *Renewable Energy*, *86*, 409–421. Retrieved from http://dx.doi.org/10.1016/j.renene.2015.08.019 doi: 10.1016/j.renene.2015.08.019

Hunt, J. C. R., Wray, a. a., & Moin, P. (1988). Eddies, streams, and convergence zones in turbulent flows. *Center for Turbulence Research, Proceedings of the Summer Program*(1970), 193–208. doi: CTR-S88

Julien, P. (2010). *Erosion and Sedimentation* (Second ed.). Cambridge University Press.

Kalitzin, G., Medic, G., Iaccarino, G., & Durbin, P. (2005). Near-wall behavior of RANS turbulence models and implications for wall functions. *Journal of Computational Physics*, *204*(1), 265–291. doi: 10.1016/j.jcp.2004.10.018

Kang, S., Chamorro, L., Hill, C., Arndt, R., & Sotiropoulos, F. (2014). Flow structure interaction around an axial-flow hydrokinetic turbine: Experiments and CFD simulations. *Journal of Physics: Conference Series*, *555*(1), 012097. Retrieved from http://stacks.iop.org/1742-6596/555/i=1/a=012097?key=crossref.f623a5fd9d208765334a313b7a21287d doi: 10.1088/1742-6596/555/1/012097

Khojasteh, D., Mousavi, S. M., Glamore, W., & Iglesias, G. (2018). Wave energy status in Asia. *Ocean Engineering*, *169*(April), 344–358. Retrieved from https://linkinghub.elsevier.com/retrieve/pii/S0029801818304323 doi: 10.1016/j.oceaneng.2018.09.034

Koh, W. X., & Ng, E. Y. (2017). A CFD study on the performance of a tidal turbine under various flow and blockage conditions. *Renewable Energy*, *107*, 124–137. doi: 10.1016/j.renene.2017.01.052

Kolekar, N., & Banerjee, A. (2015). Performance characterization and placement of a marine hydrokinetic turbine in a tidal channel under boundary proximity and blockage effects. *Applied Energy*, *148*, 121–133. Retrieved from http://dx.doi.org/10.1016/j.apenergy.2015.03.052 doi: 10.1016/j.apenergy.2015.03.052

Lewis, M., Neill, S. P., Robins, P. E., & Hashemi, M. R. (2015). Resource assessment for future generations of tidal-stream energy arrays. *Energy*. doi: 10.1016/j.energy.2015.02.038

Li, Y., & Çalişal, S. M. (2010). Numerical analysis of the characteristics of vertical axis tidal current turbines. *Renewable Energy*, *35*(2), 435–442.

Magagna, D., & Uihlein, A. (2015). Ocean energy development in Europe: Current status and future perspectives. *International Journal of Marine Energy*, *11*, 84–104. doi: 10.1016/j.ijome.2015.05.001

Maganga, F., Germain, G., King, J., Pinon, G., & Rivoalen, E. (2010). Experimental characterisation of flow effects on marine current turbine behaviour and on its wake properties. *IET Renewable Power Generation*, *4*(6), 498. Retrieved from www.ietdl.orghttp://digital-library.theiet.org/content/journals/10.1049/iet-rpg.2009.0205 doi: 10.1049/iet-rpg.2009.0205

Malki, R., Masters, I., Williams, A. J., & Nick Croft, T. (2014). Planning tidal stream turbine array layouts using a coupled blade element momentum - computational fluid dynamics model. *Renewable Energy*, *63*, 46–54. Retrieved

from http://dx.doi.org/10.1016/j.renene.2013.08.039 doi: 10.1016/j.renene.2013.08.039

Masters, I., Chapman, J., Willis, M., & Orme, J. (2011). A robust blade element momentum theory model for tidal stream turbines including tip and hub loss corrections. *Journal of Marine Engineering & Technology*, *10*(1), 25–35.

Masters, I., Williams, A., Croft, T. N., Togneri, M., Edmunds, M., Zangiabadi, E., ... Karunarathna, H. (2015). A comparison of numerical modelling techniques for tidal stream turbine analysis. *Energies*, *8*(8), 7833–7853. doi: 10.3390/en8087833

Musa, M., Hill, C., Sotiropoulos, F., & Guala, M. (2018). Performance and resilience of hydrokinetic turbine arrays under large migrating fluvial bedforms. *Nature Energy*. Retrieved from http://www.nature.com/articles/s41560-018-0218-9 doi: 10.1038/s41560-018-0218-9

Mycek, P., Gaurier, B., Germain, G., Pinon, G., & Rivoalen, E. (2013). Numerical and experimental study of the interaction between two marine current turbines. *International Journal of Marine Energy*, *1*, 70–83. doi: 10.1016/j.ijome.2013.05.007

Mycek, P., Gaurier, B., Germain, G., Pinon, G., & Rivoalen, E. (2014b, jun). Experimental study of the turbulence intensity effects on marine current turbines behaviour. Part I: One single turbine. *Renewable Energy*, *66*, 729–746. Retrieved from https://linkinghub.elsevier.com/retrieve/pii/S096014811400007X doi: 10.1016/j.renene.2013.12.036

Mycek, P., Gaurier, B. B. B., Germain, G. G. G., Pinon, G. G. G., & Rivoalen, E. (2014a). Experimental study of the turbulence intensity effects on marine current turbines behaviour. Part II: Two interacting turbines. *Renewable Energy*, *66*(June), 729–746. Retrieved from http://dx.doi.org/10.1016/j.renene.2013.12.048http://dx.doi.org/10.1016/j.renene.2013.12.036 doi: 10.1016/j.renene.2013.12.036

Myers, L., Bahaj, B., Germain, G., & Giles, J. (n.d.). *Flow boundary interaction effects for marine current energy conversion devices* (Tech. Rep.). Retrieved from www.energy.soton.ac.uk

Nash, S., & Phoenix, A. (2017). A review of the current understanding of the hydro-environmental impacts of energy removal by tidal turbines. *Renewable and Sustainable Energy Reviews*, *80*(June), 648–662. Retrieved from http://dx.doi.org/10.1016/j.rser.2017.05.289 doi: 10.1016/j.rser.2017.05.289

Nishino, T., & Willden, R. H. J. (2012). The efficiency of an array of tidal turbines partially blocking a wide channel. *Journal of Fluid Mechanics*, *708*, 596–606. doi: 10.1017/jfm.2012.349

Olczak, A., Stallard, T., Feng, T., & Stansby, P. K. (2016). Comparison of a RANS blade element model for tidal turbine arrays with laboratory scale measurements of wake velocity and rotor thrust. *Journal of Fluids and Structures*, *64*, 87–106. Retrieved from http://dx.doi.org/10.1016/j.jfluidstructs.2016.04.001 doi: 10.1016/j.jfluidstructs.2016.04.001

Paboeuf, S., Yen Kai Sun, P., Macadré, L.-M., Malgorn, G., Yen, P., Sun, K., ... Malgorn, G. (2016, jun). Power Performance Assessment of the Tidal Turbine Sabella D10 Following IEC62600-200. In *Volume 6: Ocean space utilization; ocean renewable energy* (Vol. 6, p. V006T09A007). ASME. Retrieved from http://proceedings.asmedigitalcollection.asme.org/pdfaccess.ashx?url=/data/conferences/asmep/89861/http://proceedings.asmedigitalcollection.asme.org/proceeding.aspx?articleid=2570928http://proceedings.asmedigitalcollection.asme.org/proceeding.aspx?doi=1 doi: 10.1115/OMAE2016-54836

Paik, J., Cristian Escauriaza, ., Sotiropoulos, F., Asce, M., Escauriaza, C., Sotiropoulos, F., ... Asce, M. (2010). Coherent structure dynamics in turbulent flows past in-stream structures: Some insights gained via numerical simulation. *Journal of Hydraulic Engineering*, *136*(12), 981–993. Retrieved from http://www.scopus.com/inward/record.url?eid=2-s2.0-78349288009{&}partnerID=40{&}md5=b877570b0785c3e5ee2b454bf7f30a9f doi:

doi:10.1061/(ASCE)HY.1943-7900.0000089

Paik, J., Escauriaza, C., & Sotiropoulos, F. (2007, apr). On the bimodal dynamics of the turbulent horseshoe vortex system in a wing-body junction. *Physics of Fluids*, *19*(4), 045107. Retrieved from http://www.scopus.com/inward/record.url?eid=2-s2.0-78349288009{&}partnerID=40{&}md5=b877570b0785c3e5ee2b454bf7f30a9fhttp://aip.scitation.org/doi/10.1063/1.2716813 doi: 10.1063/1.2716813

Paik, J., Sotiropoulos, F., & Porté-Agel, F. (2009). Detached eddy simulation of flow around two wall-mounted cubes in tandem. *International Journal of Heat and Fluid Flow*, *30*(2), 286–305. Retrieved from http://dx.doi.org/10.1016/j.ijheatfluidflow.2009.01.006 doi: 10.1016/j.ijheatfluidflow.2009.01.006

Parsheh, M., Sotiropoulos, F., & Porté-Agel, F. (2010). Estimation of Power Spectra of Acoustic-Doppler Velocimetry Data Contaminated with Intermittent Spikes. *Journal of Hydraulic Engineering*, *136*(6), 368–378. Retrieved from http://ascelibrary.org/doi/10.1061/{%}28ASCE{%}29HY.1943-7900.0000202 doi: 10.1061/(ASCE)HY.1943-7900.0000202

Rahimian, M., Walker, J., & Penesis, I. (2018). Performance of a horizontal axis marine current turbine– A comprehensive evaluation using experimental, numerical, and theoretical approaches. *Energy*, *148*, 965–976. Retrieved from http://linkinghub.elsevier.com/retrieve/pii/S0360544218302329 doi: 10.1016/j.energy.2018.02.007

Rao, S., Xue, H., Bao, M., & Funke, S. (2016). Determining tidal turbine farm efficiency in the Western Passage using the disc actuator theory. *Ocean Dynamics*, *66*(1), 41–57. doi: 10.1007/s10236-015-0906-y

Rourke, F. O., Boyle, F., & Reynolds, A. (2010). Marine current energy devices: Current status and possible future applications in Ireland. *Renewable and Sustainable Energy Reviews*, *14*(3), 1026–1036. doi: 10.1016/j.rser.2009.11.012

Schluntz, J., & Willden, R. H. (2015). The effect of blockage on tidal turbine rotor design and performance. *Renewable Energy*, *81*, 432–441. Retrieved from http://dx.doi.org/10.1016/j.renene.2015.02.050 doi: 10.1016/j.renene.2015.02.050

Shen, W. Z., Mikkelsen, R., Sørensen, J. N., & Bak, C. (2005). Tip loss corrections for wind turbine computations. *Wind Energy: An International Journal for Progress and Applications in Wind Power Conversion Technology*, *8*(4), 457–475.

Shives, M., & Crawford, C. (2016). Adapted two-equation turbulence closures for actuator disk RANS simulations of wind & tidal turbine wakes. *Renewable Energy*, *92*, 273–292. doi: 10.1016/j.renene.2016.02.026

Smirnov, A., Shi, S., & Celik, I. (2001). Random Flow Generation Technique for Large Eddy Simulations and Particle-Dynamics Modeling. *Journal of Fluids Engineering*, *123*(2), 359. doi: 10.1115/1.1369598

Spalart, P., & Allmaras, S. (1992). A one-equation turbulence model for aerodynamic flows. In *30th aerospace sciences meeting and exhibit* (p. 439).

Spalart, P. R. (1997). Comments on the feasibility of LES for wings, and on a hybrid RANS/LES approach. In *Proceedings of first afosr international conference on dns/les.*

Spalart, P. R. (2009). Detached-Eddy Simulation. *Annual Review of Fluid Mechanics*, *41*(1), 181–202. Retrieved from http://www.annualreviews.org/doi/10.1146/annurev.fluid.010908.165130 doi: 10.1146/annurev.fluid.010908.165130

Stallard, T., Collings, R., Feng, T., & Whelan, J. (2013a). Interactions between tidal turbine wakes: Experimental study of a group of three-bladed rotors. *Philosophical Transactions of the Royal Society A*, *371*(1985), 1471–2962.

Stallard, T., Collings, R., Feng, T., & Whelan, J. (2013b). Interactions between tidal turbine wakes: experimental study of a group of three-bladed rotors. *Philosophical Transactions of the Royal Society A: Mathematical, Physical and Engineering Sciences*, *371*(1985), 20120159–20120159. Retrieved from http://rsta.royalsocietypublishing.org/cgi/doi/10.1098/rsta.2012.0159 doi: 10.1098/rsta.2012.0159

Tedds, S. C., Owen, I., & Poole, R. J. (2014). Near-wake characteristics of a model horizontal axis tidal stream turbine. *Renewable Energy*, *63*, 222–235. Retrieved from http://dx.doi.org/10.1016/j.renene.2013.09.011 doi: 10.1016/j.renene.2013.09.011

The Executive Committee of Ocean Energy Systems. (2015). 2014 Annual Report. *Ocean Energy Systems*, 1–148. Retrieved from http://report2014.ocean-energy-systems.org/documents/OES-Annual-Report-2014/ doi: 10.1017/S0001972000001765

Turnock, S. R., Phillips, A. B., Banks, J., & Nicholls-Lee, R. (2011). Modelling tidal current turbine wakes using a coupled RANS-BEMT approach as a tool for analysing power capture of arrays of turbines. *Ocean Engineering*, *38*(11-12), 1300–1307. Retrieved from http://dx.doi.org/10.1016/j.oceaneng.2011.05.018 doi: 10.1016/j.oceaneng.2011.05.018

U.S. Energy Information Administration. (2016). *International Energy Outlook 2016* (Vol. 0484(2016)) (No. May 2016). Retrieved from www.eia.gov/forecasts/ieo/pdf/0484(2016).pdf doi: www.eia.gov/forecasts/ieo/pdf/0484(2016).pdf

Valente, A., Iribarren, D., & Dufour, J. (2017). Harmonised life-cycle global warming impact of renewable hydrogen. *Journal of Cleaner Production*, *149*, 762–772. Retrieved from http://dx.doi.org/10.1016/j.jclepro.2017.02.163 doi: 10.1016/j.jclepro.2017.02.163

van Rijn, L. C. (1984, nov). Sediment Transport, Part II:

Suspended Load Transport. *Journal of Hydraulic Engineering*, *110*(11), 1613–1641. Retrieved from https://doi.org/10.1061/(ASCE)0733-9429(1984)110:11(1613)http://ascelibrary.org/doi/10.1061/{%}28ASCE{%}290733-9429{%}281984{%}29110{%}3A11{%}281613{%}29 doi: 10.1061/(ASCE)0733-9429(1984)110:11(1613)

Vazquez, A., & Iglesias, G. (2015). Device interactions in reducing the cost of tidal stream energy. *Energy Conversion and Management*, *97*, 428–438. Retrieved from http://dx.doi.org/10.1016/j.enconman.2015.03.044 doi: 10.1016/j.enconman.2015.03.044

Yuce, M. I., & Muratoglu, A. (2015, mar). Hydrokinetic energy conversion systems: A technology status review. *Renewable and Sustainable Energy Reviews*, *43*(9), 72–82. Retrieved from http://dx.doi.org/10.1016/j.rser.2014.10.037https://linkinghub.elsevier.com/retrieve/pii/S1364032114008624 doi: 10.1016/j.rser.2014.10.037

Zhou, Z., Benbouzid, M., Charpentier, J. F., Scuiller, F., & Tang, T. (2017). *Developments in large marine current turbine technologies – A review* (Vol. 71). doi: 10.1016/j.rser.2016.12.113

Zhou, Z., Scuiller, F., Charpentier, J. F., Benbouzid, M., & Tang, T. (2014). An up-to-date review of large marine tidal current turbine technologies. *Proceedings - 2014 International Power Electronics and Application Conference and Exposition, IEEE PEAC 2014*, 480–484. doi: 10.1109/PEAC.2014.7037903

APPENDIX

A. DES-BEM ALGORITHM

As model input parameter the exact rotor location is requested: x-axis range, rotor center node, and rotor and hub radius. With this values the turbine volume V can be calculated, and withing V the algorithm of Figure A.1 is applied to every node.

At the beginning of each time step the local velocity for every node inside V is obtained. If the distance between rotor center and node is less than hub radius, i.e. no is inside hub region, a zero velocity is applied in order to represent the drag induced on the flow by hub, just as explained in section 2.2.2. For the rest of nodes the forces applied by the blades over flow is obtained by BEM approach. Before passing the forces to the flow solver, C_P and C_T are printed saved into a file.

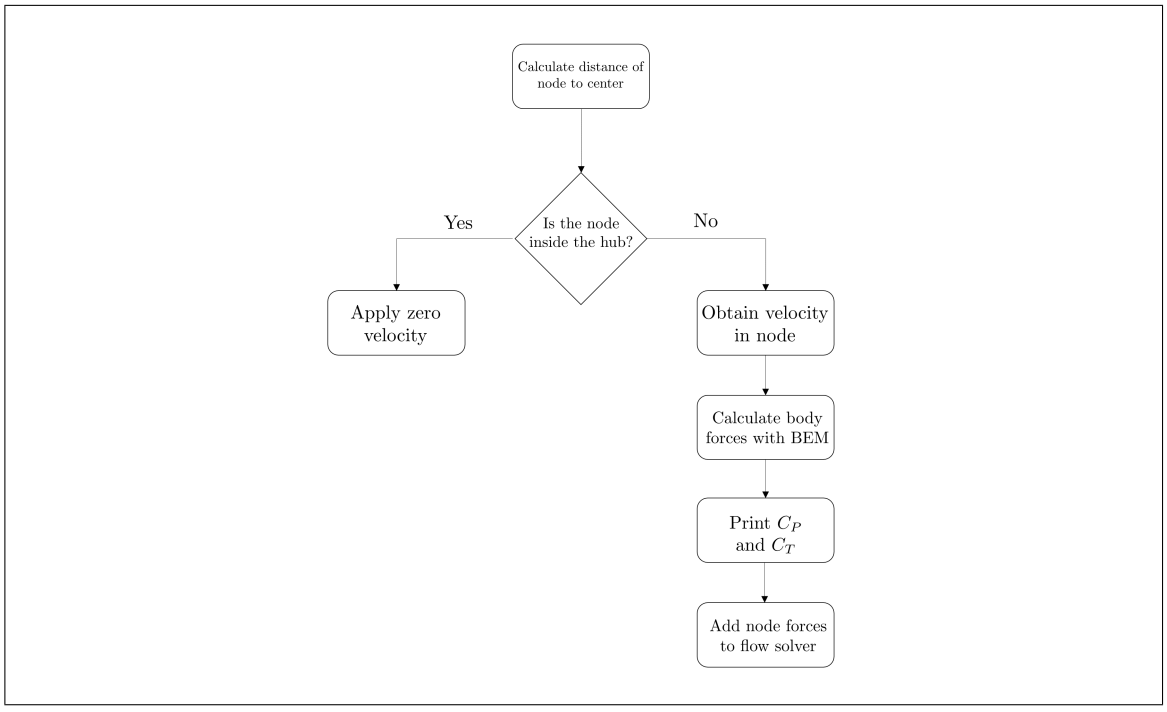

Figure A.1. DES-BEM simplified algorithm to apply turbine blade forces estimated by BEM to flow solver.

B. BLADE ELEMENT MOMENTUM THEORY

As explained in section 2.2.2, lift and drag forces per span unit length are calculated as:

$$f_L = \frac{1}{2}\rho c(r) U_{rel}^2 C_L(\alpha, Re) \tag{B.1}$$

$$f_D = \frac{1}{2}\rho c(r) U_{rel}^2 C_D(\alpha, Re) \tag{B.2}$$

where ρ is fluid density, U_{rel} is the relative speed between the blades and fluid, and $c(r)$ is the blade chord length at a radial distance r from the rotor center. Lift (C_L) and Drag (C_D) coefficients are functions of the blade geometry, the angle of attack α, and the local Reynolds number over the blade. The values of C_L and C_D depends of each turbine and usually are tabulated for different angles of attack and Reynolds numbers.

For a node inside the turbine volume V, and located at a radial distance r from the disk center, relative velocity U_{rel} is calculated as:

$$U_{rel} = \sqrt{u^2 + (r\Omega_{rel})^2} \tag{B.3}$$

where u is the node local instantaneous longitudinal velocity component and Ω_{rel} is the relative rotational velocity between the blade and the fluid. The rotational velocity is calculated as:

$$\Omega_{rel} = r\Omega + v\sin(\theta) - w\cos(\theta) \tag{B.4}$$

where θ is the azimuthal angle between the mesh node and the horizontal plane as shown in Figure 2.4, v and w are the local transverse and vertical velocity components, respectively, and Ω is the turbine rotational velocity.

The relative flow angle ϕ, shown in Figure B.1, is used to calculate the local angle of attack. Φ can be obtained by

$$\phi = \tan^{-1}\left(\frac{u}{r\Omega_{rel}}\right) \tag{B.5}$$

After this angle is calculated, the local angle of attack needed to get C_L and C_D is obtained

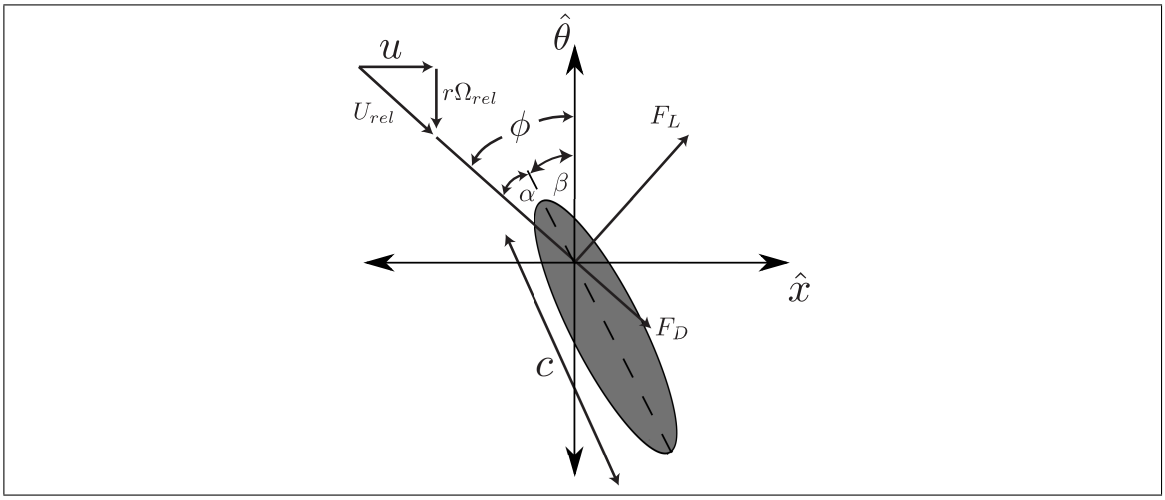

Figure B.1. Blade cut view of the variables involved in the lift and drag decomposition of BEM

by

$$\alpha(r) = \phi - \beta(r) \tag{B.6}$$

where β is the local twist angle, defined as the angle variation of the blade from its origin position at the blade root. This angle is a function of r and depends on turbine blade design.

To incorporate f_L and f_D into the flow solver they must be transformed into body forces. Creech et al. (2015) propose

$$F_L = \eta(x^*) \left(\frac{N_{blades}}{2\pi r} \right) f_L \tag{B.7}$$

$$F_D = \eta(x^*) \left(\frac{N_{blades}}{2\pi r} \right) f_D \tag{B.8}$$

where N_{blades} is the number of blades and $\eta(x^*)$ is a Gaussian function used to distribute the forces axially inside the turbine volumes.

The function $\eta(x^*)$ depends on the longitudinal distance between the mesh node and the disk center, x^*, and is defined as:

$$\eta(x^*) = \frac{1}{\sqrt{2\pi\sigma^2}} e^{-\frac{1}{2}\left(\frac{x^*}{\sigma}\right)} \tag{B.9}$$

The body forces calculated are then decomposed into axial and azimuthal components acting on the fluid.

$$F_x = -\left(F_L \cos(\phi) + F_D \sin(\phi)\right) \tag{B.10}$$

$$F_{azim} = -\left(F_L \sin(\phi) - F_D \cos(\phi)\right) \tag{B.11}$$

The azimuthal component is then written in terms of its lateral and vertical directions

$$F_y = -\sin(\theta) F_{azim} \tag{B.12}$$

$$F_z = \cos(\theta) F_{azim} \tag{B.13}$$

The resulting forces are then non-dimensionalized and passed to the source terms of the DES flow solver.

C. UNSTEADY INLET GENERATOR

In order to create a realistic inlet velocity profiles we used the Random Flow Generator (RFG) technique proposed by Smirnov et al.(2001). The steps to use the method are the following:

(1) Diagonalize the velocity correlation tensor:

For any anisotropic velocity correlation tensor

$$r_{ij} = \overline{u_i u_j} \tag{C.1}$$

obtain an orthonormal transformation tensor a_{ij} for diagonalizing r_{ij}

$$a_{mi} a_{nj} r_{ij} = d_{mn} c^2_{(n)} \tag{C.2}$$

$$a_{ik} a_{kj} = \delta_{ij} \tag{C.3}$$

In the new coordinate system represented by the tensor a_{ij}, the coefficients $c_n = \{c_1,\, c_2,\, c_3\}$ represent the fluctuating velocities $(u',\, v',\, w')$.

(2) Generate a transient flow-field:

For every point and time $(\vec{x}, t)$ where the RFG technique will be applied use the following function for generating a velocity series $v_i(\vec{x}, t)$:

$$v_i(\vec{x}, t) = \sqrt{\frac{2}{N}} \sum_{n=1}^{N} \left[p_i^n \cos\left(\tilde{k}_j^n \tilde{x}_j + \omega_n \tilde{t} \right) \right] \tag{C.4}$$

$$\tilde{x}_j = \frac{x_j}{l}, \tilde{t} = \frac{t}{\tau}, c = \frac{l}{\tau}, \tilde{k}_j^n = k_j^n \frac{c}{c_{(j)}} \tag{C.5}$$

$$p_i^n = \epsilon_{ijm} \zeta_j^n k_m^n, q_i^n = \epsilon_{ijm} \xi_j^n k_m^n \tag{C.6}$$

$$\zeta_i^n, \xi_i^n, \omega_n \in N(0,1), k_i^n \in N(0, 1/2) \tag{C.7}$$

where l, τ are length- and time-scales of turbulence, ϵ_{ijk} is the permutation tensor and $N(M, \sigma)$ is a normal distribution with M and σ as mean and standard deviation, respectively. The numbers k_j^n, ω_n are sample of n wave-numbers and frequencies,

respectively, of the turbulence spectrum

$$E(k) = 16\left(\frac{2}{\pi}\right)^{1/2} k^4 \exp\left(-2k^2\right) \tag{C.8}$$

(3) Scale the flow-field:

To obtain a new flow-field u_i in the original coordinate system we apply a the following scaling and orthogonal transformation to the results obtained above:

$$w_i = c_{(i)} v_{(i)} \tag{C.9}$$

$$u_i = a_{(ik)} w_{(k)} \tag{C.10}$$

In our configuration we assume an isotropic correlation tensor at the inlet, with turbulent intensity obtained from upstream measurements with ADV profiler. The sampling number was set to $N = 1000$ as Smirnov et al. (2001)) did. The characteristic length scale l for every mesh node in the inlet was defined as 0.1 times coefficient of the distance from node to wall used in DES.

$$l = 0.1 \min\left\{d, 0.65\Delta\right\} \tag{C.11}$$

where d is the distance to the closest wall and Δ is the largest grid spacing nearest to the node $\Delta = max\left\{\Delta_x, \Delta_y, \Delta_z\right\}$. The time scale was built using TI_x as a reference:

$$\tau = \frac{l}{TI_x} \tag{C.12}$$